



Increased circulation time of *Plasmodium falciparum* underlies persistent asymptomatic infection in the dry season

Carolina M. Andrade^{ID 1}, Hannah Fleckenstein¹, Richard Thomson-Luque^{ID 1}, Sariatou Doumbo², Nathalia F. Lima¹, Carrie Anderson¹, Julia Hibbert¹, Christine S. Hopp^{ID 3}, Tuan M. Tran^{ID 4}, Shaping Li³, Moussa Niangaly², Hamidou Cisse^{ID 2}, Didier Doumtabe², Jeff Skinner³, Dan Sturdevant⁵, Stacy Ricklefs⁵, Kimmo Virtaneva^{ID 5}, Muhammad Asghar^{6,7}, Manijeh Vafa Homann^{ID 6,7}, Louise Turner^{8,9}, Joana Martins¹⁰, Erik L. Allman¹¹, Marie-Ester N'Dri¹², Volker Winkler¹³, Manuel Llinás^{ID 11,14}, Catherine Lavazec¹², Craig Martens⁵, Anna Färnert^{6,7}, Kassoum Kayentao², Aissata Ongoiba², Thomas Lavstsen^{8,9}, Nuno S. Osório^{ID 10}, Thomas D. Otto^{ID 15}, Mario Recker^{ID 16}, Boubacar Traore², Peter D. Crompton³ and Silvia Portugal^{ID 1,17,18}

The dry season is a major challenge for *Plasmodium falciparum* parasites in many malaria endemic regions, where water availability limits mosquito vectors to only part of the year. How *P. falciparum* bridges two transmission seasons months apart, without being cleared by the human host or compromising host survival, is poorly understood. Here we show that low levels of *P. falciparum* parasites persist in the blood of asymptomatic Malian individuals during the 5- to 6-month dry season, rarely causing symptoms and minimally affecting the host immune response. Parasites isolated during the dry season are transcriptionally distinct from those of individuals with febrile malaria in the transmission season, coinciding with longer circulation within each replicative cycle of parasitized erythrocytes without adhering to the vascular endothelium. Low parasite levels during the dry season are not due to impaired replication but rather to increased splenic clearance of longer-circulating infected erythrocytes, which likely maintain parasitemias below clinical and immunological radar. We propose that *P. falciparum* virulence in areas of seasonal malaria transmission is regulated so that the parasite decreases its endothelial binding capacity, allowing increased splenic clearance and enabling several months of subclinical parasite persistence.

The mosquito-borne *P. falciparum* parasite is responsible for over 200 million malaria cases annually, and in 2018 it killed nearly 400,000 individuals, most of whom were African children under 5 years of age¹. *P. falciparum* causes disease while multiplying asexually within red blood cells (RBCs) and exporting its variant surface antigens (VSAs) to the RBC surface. VSAs mediate adhesion to vascular endothelium, thereby helping the parasite avoid splenic clearance^{2,3}. During each ~48-h replicative cycle in RBCs, *P. falciparum* follows a regulated transcriptional pattern, starting from the invading merozoite, through the ring and trophozoite stages and to the multinucleated schizont^{4,5}, which yields

16–32 new merozoites. In parallel with a predictable transcriptional pattern, the parasite develops a network of membrane structures⁶ in the infected RBC (iRBC), and, at the trophozoite stage, the host cell membrane presents knobs⁷ exposing parasite-derived *P. falciparum* erythrocyte membrane protein 1 (PfEMP1), encoded by the multigene family *var*⁸. *var* genes are expressed in a monoallelic fashion, coding for PfEMP1s that bind host endothelial cell receptors, with different binding phenotypes associating with varying virulence and pathological outcomes⁹. In Mali and many African regions, malaria cases are restricted to the rainy season when the mosquitoes transmitting *P. falciparum* are present¹⁰, and

¹Center for Infectious Diseases, Parasitology, Heidelberg University Hospital, Heidelberg, Germany. ²Mali International Center of Excellence in Research, University of Sciences, Techniques and Technologies of Bamako, Bamako, Mali. ³Laboratory of Immunogenetics, National Institute of Allergy and Infectious Diseases, National Institutes of Health, Rockville, MD, USA. ⁴Division of Infectious Diseases, Indiana University School of Medicine, Indianapolis, IN, USA.

⁵Rocky Mountain Laboratory Research Technologies Section, Genomics Unit, National Institute of Allergy and Infectious Diseases, National Institutes of Health, Hamilton, MT, USA. ⁶Department of Medicine Solna, Division of Infectious Diseases, Karolinska Institutet, Stockholm, Sweden. ⁷Department of Infectious Diseases, Karolinska University Hospital, Stockholm, Sweden. ⁸Department of Immunology and Microbiology, Centre for Medical Parasitology, Faculty of Health and Medical Sciences, University of Copenhagen, Copenhagen N, Denmark. ⁹Department of Infectious Diseases, Copenhagen University Hospital (Rigshospitalet), Copenhagen, Denmark. ¹⁰Life and Health Sciences Research Institute (ICVS), School of Medicine, University of Minho, Portugal and ICVS/3B's -PT Government Associate Laboratory, Braga, Portugal. ¹¹Department of Biochemistry and Molecular Biology, Huck Center for Malaria Research, The Pennsylvania State University, State College, PA, USA. ¹²Université de Paris, Institut Cochin, Paris, France. ¹³Institute of Global Health, Heidelberg University Hospital, Heidelberg, Germany. ¹⁴Department of Chemistry, The Pennsylvania State University, State College, PA, USA. ¹⁵Institute of Infection, Immunity & Inflammation, MVL, University of Glasgow, Glasgow, UK. ¹⁶Centre for Mathematics & the Environment, University of Exeter, Penryn Campus, Penryn, UK. ¹⁷German Center for Infection Research (DZIF), Heidelberg, Heidelberg, Germany. ¹⁸Present address: Max Planck Institute for Infection Biology, Berlin, Germany. e-mail: portugal@mpib-berlin.mpg.de

subclinical *P. falciparum* infections can persist throughout the dry season, enabling the parasite to bridge transmission seasons several months apart^{11–13}. We recently showed that, although *P. falciparum*-specific humoral immunity is higher in subclinical *P. falciparum* carriers in the dry season, it decreases similarly from its beginning to its end in carriers and non-carriers¹³, suggesting that chronic low parasitemia in endemic settings might not maintain or boost malaria immunity. Although much is known about immune responses to clinical malaria, and, to some extent, to subclinical infections during the transmission season¹⁴, the effect on immunity of subclinical *P. falciparum* persistence in the dry season has not been extensively studied. Host survival during the dry months is essential for resuming *P. falciparum* transmission in the ensuing rainy season; thus, the parasite has likely evolved strategies to prevent potentially fatal host pathology and assure persistence during mosquito-free periods. In this study, we addressed the host and parasite features that associate with parasite persistence between two transmission seasons and provide insights into the complex interaction among *P. falciparum*, its human hosts and the surrounding environment. By comparing parasites from the dry season to malaria-causing parasites in the transmission season, we show that, despite inducing a minimal immune response and conserving its replication ability, *P. falciparum* dry season parasitemias can be maintained low by splenic clearance of a large proportion of iRBCs that circulate longer than observed in clinical malaria cases.

Results

***P. falciparum* persists during the dry season.** In a cohort study in Kalifabougou, Mali, we followed ~600 individuals from 3 months to 45 years of age during 2017 and 2018. As reported earlier¹³, clinical episodes of malaria (temperature $\geq 37.5^{\circ}\text{C}$, $\geq 2,500$ asexual parasites per μl and no other clinically discernible cause of fever) were largely restricted to the transmission seasons (June–December), whereas nearly all individuals remained free of symptomatic malaria during the intervening dry seasons (January–May). Specifically, 386 and 347 febrile malaria cases were diagnosed during the 2017 and 2018 rainy seasons, respectively, whereas only 12 and five febrile malaria episodes occurred during the dry seasons (Fig. 1a and Extended Data Fig. 1). Despite the very low incidence of clinical malaria in the dry season, we consistently observed 10–20% prevalence of subclinical *P. falciparum* infections during this time. Analyzing over 400 individuals with paired data at the beginning (January) and end (May) of each dry season, we found that 20% of individuals were *P. falciparum* polymerase chain reaction (PCR)⁺ both in January 2017 and January 2018, and 15% and 12% of individuals were *P. falciparum* PCR⁺ at the end of the 2017 and 2018 dry seasons, respectively (Fig. 1b). Older children and young adults carried subclinical *P. falciparum* more frequently than young children at the end of the dry season (Fig. 1c and Extended Data Fig. 1), as reported earlier for this cohort¹³. Also, as previously reported, we observed that subclinical *P. falciparum* carriers at the end of the dry season were very likely to have been infected since its beginning (January 2017 or January 2018), whereas uninfected individuals at the beginning of a dry season remained uninfected until its end (Fig. 1b). The odds ratios (ORs) of maintaining the same infection status through each entire dry season were OR = 90.9 (95% confidence interval (CI) (38.6, 213.8), $P < 0.0001$) in 2017 and OR = 43.5 (95% CI (17.5, 107.5), $P < 0.0001$) in 2018 (Supplementary Table 1). Consistent with the continued absence of clinical malaria during the dry season, parasitemias of subclinical carriers determined by RT-qPCR and flow cytometry were found to remain low, or, in some individuals, decline as the dry season progressed, whereas clinical cases of malaria in the wet season presented with high parasite burdens (Fig. 1d). Interestingly, the very few clinical malaria cases occurring during the dry seasons had significantly lower parasitemias than those presented by the same individuals in clinical cases during the ensuing rainy seasons (Extended Data Fig. 2).

***P. falciparum* induces a minimal immune response during the dry season.** To test the hypothesis that host immunity might contribute to the suppression of parasitemia during the dry season, we compared the immune responses of subclinical carriers of *P. falciparum* (May⁺) versus non-infected children (May⁻). We profiled individuals between 7 and 17 years of age, as this was the group in which most subclinical infections were detected, for serological markers of inflammation and cytokines, circulating immune cells and humoral responses to *P. falciparum* VSAs of age- and gender-matched children who did or did not carry *P. falciparum* during the dry season, detected retrospectively by PCR. Inflammation markers previously reported to be elevated in clinical cases of malaria, such as C-reactive protein (CRP)¹⁵, von Willebrand factor (vWF)¹⁶ and hepcidin¹⁷, were quantified in plasma samples obtained at the beginning (January) and end (May) of the dry season. None of the three markers was significantly different in subclinical carriers compared to uninfected children at either time point (Fig. 2a). We complemented these serological analyses with a multiplex bead array to detect 32 cytokines and chemokines and observed no differences between children with or without *P. falciparum* at the end of the dry season (May) in all but one of the quantified analytes (Supplementary Table 2). Only CXCL1, a pro-inflammatory chemokine known to recruit neutrophils, which has thus far not been associated with malaria in the clinical setting, was significantly increased in children with *P. falciparum*-persistent parasitemias at the end of the dry season (Fig. 2b). In contrast, CCL3, IL-10, IL-6 and IL-1 β , previously associated with clinical malaria^{18–20}, were similar in the plasma of infected versus uninfected children at the end of the dry season (Fig. 2b and Supplementary Table 2). We next quantified the proportions of major leucocyte populations from thawed peripheral blood mononuclear cells (PBMCs) collected at the end of the dry season from children with or without subclinical *P. falciparum* (gating strategy in Extended Data Fig. 3). We observed that monocytes, T cells, B cells and natural killer (NK) cell sub-populations were not significantly different between children who carried (May⁺) or did not carry (May⁻) *P. falciparum* (Fig. 2c and Extended Data Fig. 4). To interrogate differences in cell function, we quantified intracellular cytokines, activation or cytotoxicity markers, transcription factors or exhaustion markers of freshly collected PBMCs from *P. falciparum* subclinically infected and non-infected children at the end of the dry season. The levels of the activation marker CD25, transcription factor T-bet or cytokine IL-2 of CD4 T cells, granzyme B of CD8 T and NK cells and exhaustion marker FCRL5 of atypical memory B cells were similar between children who carried or did not carry *P. falciparum* (Fig. 2d and Supplementary Table 3). We further questioned whether memory B cells (MBCs, defined as CD19⁺, CD10⁻ and CD21⁻ and CD27^{+ or -} or CD21⁺ and CD27⁺; gating strategy in Extended Data Fig. 3) specific for *P. falciparum* were affected in subclinical carriers compared to non-infected individuals at the end of the dry season. Using biotinylated *P. falciparum* blood stage antigens apical membrane antigen 1 (AMA-1) and merozoite surface protein 1 (MSP1)²¹, we quantified AMA-1- or MSP1-specific MBCs in children who carried *P. falciparum* parasites and non-infected children at the end of the dry season. We found that the proportion of class-switched *P. falciparum*-specific MBCs (AMA1⁺ or MSP1⁺IgG⁺IGM⁻ MBCs) was significantly increased in subclinical carriers at the end of the dry season, whereas no such difference was found in the non-class-switched MBC population (AMA1⁺ or MSP1⁺IgG⁻IGM⁺ MBCs) (Fig. 2e). Within the IgG⁺ MBC sub-populations, we did not observe differences between *P. falciparum* carriers and uninfected individuals at the end of the dry season in *P. falciparum*-specific classical and atypical MBCs, but we detected increased *P. falciparum*-specific activated MBCs in subclinical carriers (Extended Data Fig. 4). Using another multiplex bead array, we quantified humoral responses of *P. falciparum* subclinical carriers and uninfected individuals, at the beginning

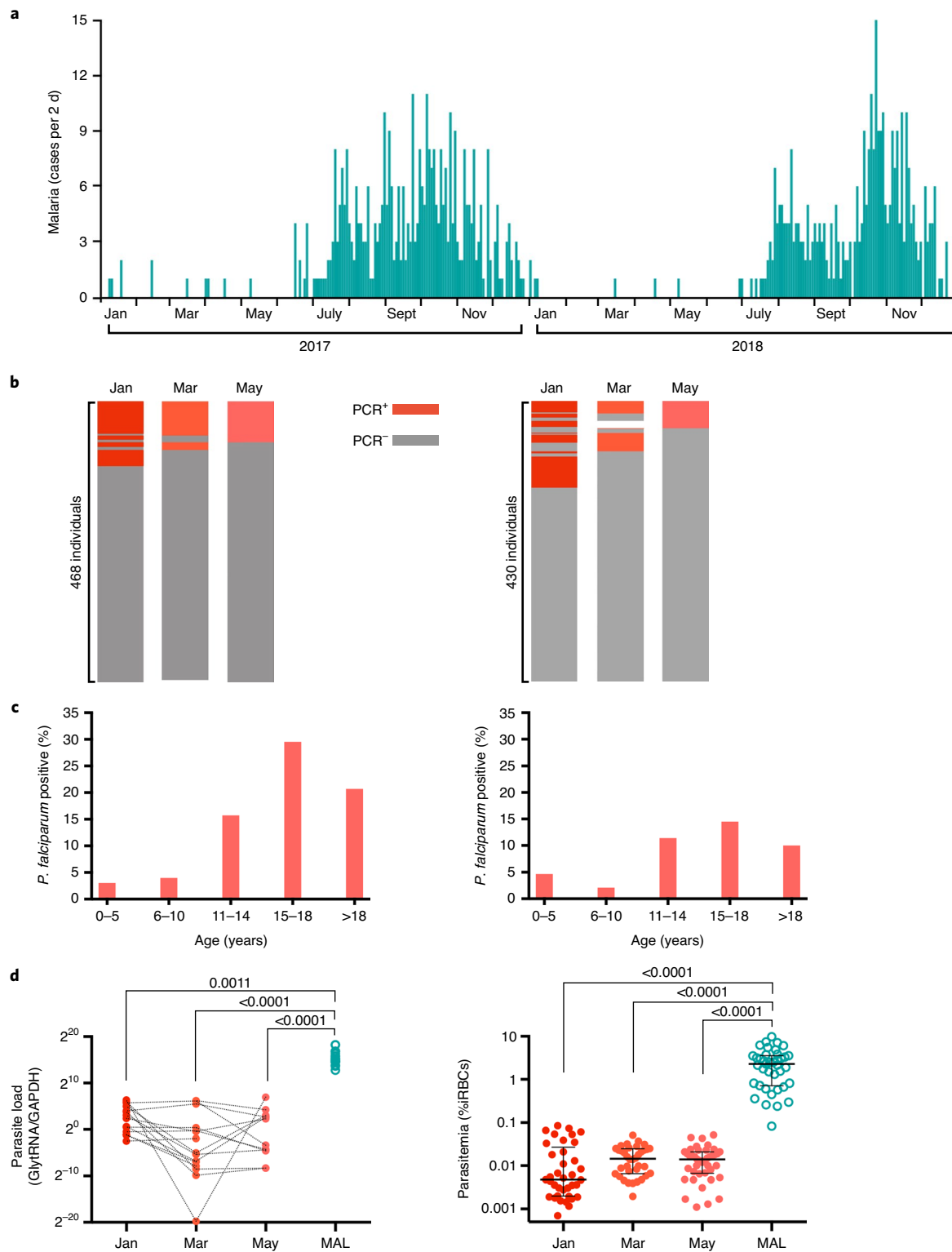


Fig. 1 | *P. falciparum* persists during the dry season. **a**, Clinical malaria frequency in a cohort of ~600 individuals aged 3 months to 45 years measured every 2 days for 2 years. Clinical malaria diagnosed by axillary temperature $\geq 37.5^{\circ}\text{C}$ and $\geq 2,500$ asexual parasites per μl of blood and no other apparent cause of fever. **b**, Prevalence of subclinical *P. falciparum* determined by PCR in paired individuals (rows) at the beginning (January), middle (March) and end (May) of two consecutive dry seasons (2017, left; 2018, right). Columns are sorted to have the same individual represented in a single row at the three time points in each dry season. **c**, Point prevalence of subclinical *P. falciparum* infection determined by PCR at the end of the dry season in May 2017 (left) and May 2018 (right) stratified by age. **d**, Parasite load detected by RT-qPCR (left) and flow cytometry (right) of RDT⁺ subclinical children at the beginning (January), mid (March) and end (May) of the dry season and children with their first clinical malaria episode (MAL) in the wet season. Parasitemia data represented as median \pm IQR; Kruskal-Wallis test with multiple comparisons. IQR, interquartile range.

and end of the dry season, to 35 domain types of the VSA multi-gene family *var*, which were grouped according to their endothelial receptor affinity (CD36, EPCR or unknown receptor) and PfEMP1 upstream promotor sequence (UPS) type (A, B or B/A types)²² (Supplementary Table 4). We observed that more subclinical carriers (May^+) than non-infected individuals (May^-) were reactive against PfEMP1 domains binding to CD36, EPCR or to unknown receptors at both time points, and also that the proportion of individuals reactive to the different PfEMP1 domains decreased over the dry season independently of individual infection status (Fig. 2f and Extended Data Fig. 4). These differences parallel our previously published data on *P. falciparum*-specific humoral responses to non-VSAs¹³, suggesting similar humoral dynamics for PfEMP1s and non-VSAs. Additionally, we observed that the magnitude of IgG reactivity to A, B or B/A types of PfEMP1 declined similarly from the beginning to the end of the dry season in children who carried subclinical infection (May^+) or were uninfected (May^-) during the dry season (Fig. 2g and Extended Data Fig. 4). Antibodies against PfEMP1 domains (Fig. 2f,g), against a large set of *P. falciparum* non-VSAs¹³ and also particularly against RBC invasion-related proteins²³ (Extended Data Fig. 4) were consistently higher in subclinical carriers compared to non-infected children at the end of the dry season, so we questioned whether the difference in humoral response at the end of the dry season could impose variance in inhibition of merozoite invasion in vitro. We tested merozoite invasion of a laboratory-adapted *P. falciparum* strain in the presence of plasma from Malian children who carried parasites or not during the dry season and evaluated the antibodies' ability to block RBC invasion. Testing complete and antibody-depleted plasma, we observed that complete Malian plasma inhibited invasion of merozoites ~fivefold more than antibody-depleted Malian plasma, whereas antibody depletion had no differential effect on the control German plasma used (Fig. 2h and Extended Data Fig. 4). Notably, however, plasma from Malian children carrying subclinical infections (May^+) or not carrying parasites (May^-) had similar ability to inhibit merozoite invasion, suggesting that the antibodies remaining elevated at the end of the dry season have no significant effect on inhibiting merozoite invasion of RBCs and are unlikely to contribute to the maintenance of low parasitemias through this mechanism.

***P. falciparum* genetic diversity is maintained throughout the year.** Next, we asked whether *P. falciparum* parasites persisting through the dry season are genetically distinct from those causing acute malaria during the transmission season. To that end, we measured the size of the merozoite surface protein 2 (*msp2*) gene, which is highly polymorphic and discriminates different *P. falciparum* genotypes^{24,25}. Through nested PCR followed by fragment analysis using capillary electrophoresis, we compared paired samples from 93 subclinical carriers at the beginning (January) and end (May) of the dry season, with 136 samples from clinical cases

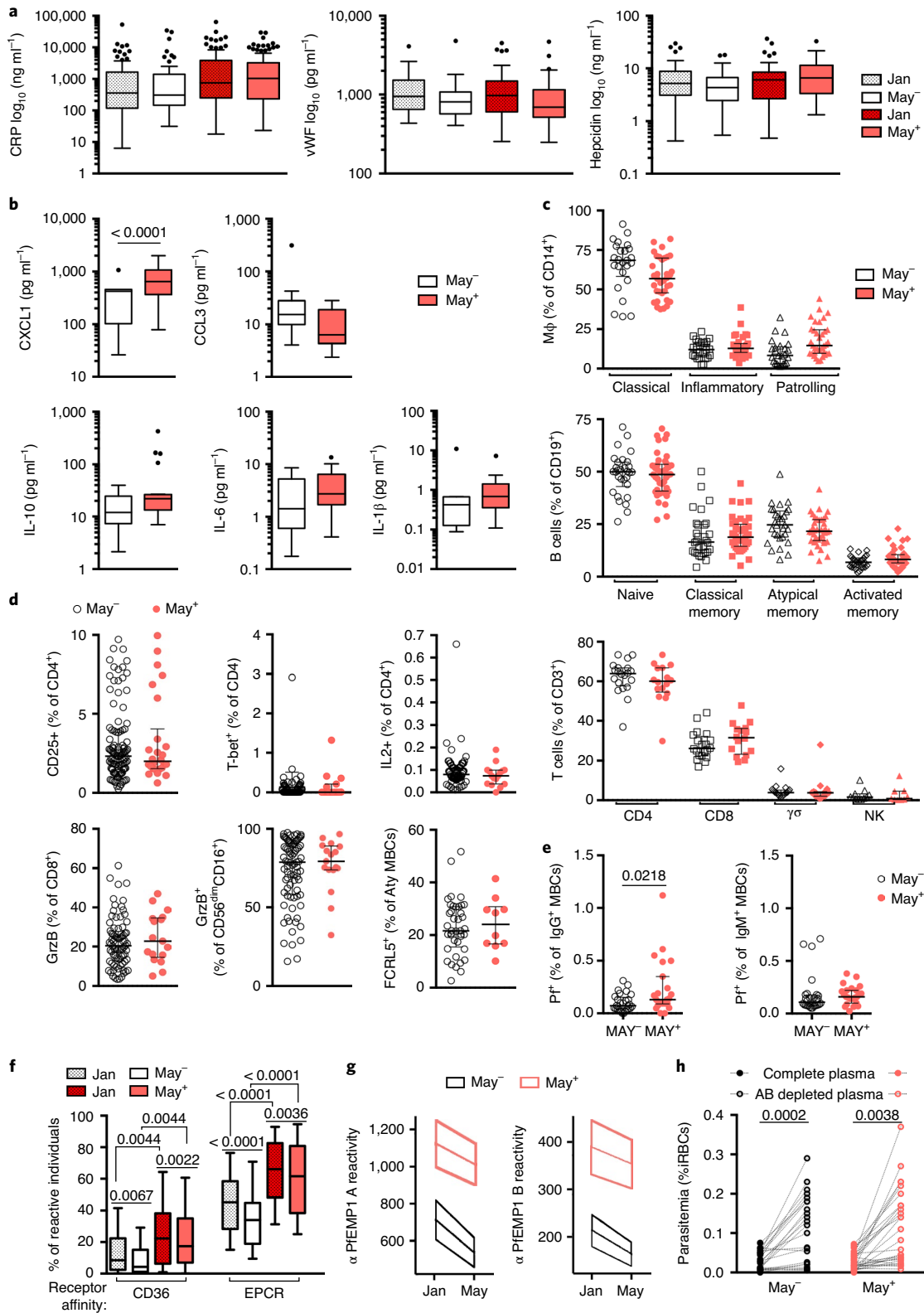
of malaria in the ensuing transmission season (MAL). The number of clones detected per individual did not significantly differ between parasites isolated during the dry season or transmission season nor did the percentage of individuals with different numbers of clones (Fig. 3a, b). Furthermore, the size and distribution of *msp2* clones identified during the dry season were similar to those isolated from clinical malaria cases during the transmission season (Fig. 3c,d), with the most frequent clone sizes being the same at any of the time points analyzed.

Transcriptome of circulating subclinical *P. falciparum* at the end of the dry season differs from that of *P. falciparum* during clinical malaria. We could not investigate the few malaria cases diagnosed in the dry season because the study protocol did not include venipuncture blood draws from clinical cases during this time. However, we performed RNA sequencing (RNA-seq) of leucocyte-depleted blood from 12 children with persistent subclinical *P. falciparum* at the end of the dry season (May) and from 12 age- and gender-matched children presenting with their first clinical malaria case in the ensuing transmission season (MAL) (Supplementary Table 5). Principal component (Fig. 4a) and unsupervised clustering (Fig. 4b) analyses showed segregation of transcription profiles based on seasonality. Differentially expressed genes (DEGs) determined at a false discovery rate threshold of 5% resulted in 1,607 DEGs, 1,131 transcripts upregulated and 476 transcripts downregulated in the dry season compared to clinical malaria samples (Fig. 4c and Supplementary Table 6). Validation of the RNA-seq data was performed by RT-qPCR of eight high-expressing and variable-in-function DEGs, and the correlation between the two methods resulted in highly significant $r^2 = 0.929$ (Fig. 4d and Supplementary Table 7). Furthermore, samples from additional children (six from the end of the dry season and 12 malaria cases during the transmission season) were used to quantify expression of three of the eight DEGs above, in parallel with the initial 24 samples, and revealed similar fold changes by RT-qPCR (Fig. 4e). We investigated similarities in the DEGs obtained in this study with those of previous reports comparing parasite physiological states and transcriptomes from a range of clinical malaria severities²⁶, or parasites causing malaria in high- versus low-transmission areas²⁷, but no enrichment was found (Extended Data Fig. 5), suggesting that singular mechanisms might be at play during the dry season. Functional and Gene Ontology analysis of the dry season DEGs revealed a significant enrichment of transcripts involved in cellular processes related with several metabolic pathways and also with phagosome, DNA replication or homologous recombination (Fig. 4f). Indeed, DEGs involved in metabolic pathways suggest that glycolysis, glycerophospholipid, purine and pyrimidine pathways were increased in parasites from the end of the dry season (May), whereas fatty acid biosynthesis appeared down-regulated compared to parasites from clinical malaria (MAL) in the wet season (Fig. 4g). Interestingly, within some pathways, there are

Fig. 2 | *P. falciparum* induces a minimal immune response during the dry season. **a**, CRP ($n=71 \text{ May}^-, 117 \text{ May}^+$), vWF ($n=33 \text{ May}^-, 51 \text{ May}^+$) and hepcidin ($n=41 \text{ May}^-, 37 \text{ May}^+$) of paired plasma samples at the beginning (January) and end (May) of the dry season from individuals carrying *P. falciparum* (May $^+$) or not (May $^-$). **b**, Plasma cytokines from children carrying or not carrying ($n=21 \text{ May}^+, 12 \text{ May}^-$) *P. falciparum* at the end of the dry season. **c**, Surface markers of frozen PBMCs from children who carried (May $^+$) or did not carry (May $^-$) *P. falciparum* at the end of the dry season. **d**, Intracellular markers of fresh PBMCs from children carrying (May $^+$) or not carrying (May $^-$) *P. falciparum* at the end of the dry season (Supplementary Table 3). **e**, *P. falciparum*-specific AMA1 $^+$ or MSP1 $^+$ MBCs in *P. falciparum* carriers or non-carriers ($n=23 \text{ May}^+, 28 \text{ May}^-$) at the end of the dry season for class-switched (IgG $^+ \text{ IGM}^-$) or non-class-switched (IgG $^- \text{ IGM}^+$) MBCs. **f**, Proportion of children with antibodies specific to PfEMP1 domains at the beginning and end of the dry season ($n=106$ January and May $^-, 112$ January and May $^+$). **g**, Magnitude of anti-PfEMP1 domains antibody response between the beginning and end of the dry season in children carrying or not carrying subclinical *P. falciparum* ($n=112$ January and May $^+, 106$ January and May $^-$). **h**, Parasitemia after invasion in complete or antibody-depleted plasma from children who carried or did not carry ($n=29 \text{ May}^+, 24 \text{ May}^-$) *P. falciparum* subclinical infections during the dry season. All data indicate median \pm IQR. (**a**) One-way ANOVA with Tukey's multiple comparisons correction; (**b**) one-way ANOVA with Sidak's multiple comparisons test. (**c, d, h**), one-sided Dunn's Kruskal-Wallis multiple comparisons test; (**e**) Mann-Whitney test; (**f**) repeated-measures one-way ANOVA (with Greenhouse-Geisser correction) for each binding receptor affinity; (**g**) slopes compared with a linear non-interaction model. (**a, b, f**) Box plots indicate median \pm IQR. Values $>1.5\times$ the IQR are plotted as individual points (Tukey's method). IQR, interquartile range.

transcripts that appear to be exceptions to the trend of upregulation or downregulation (Fig. 4g); however, we observe that these particular transcripts also present exceptional patterns of expression within the 48-h intraerythrocytic developmental cycle compared to other pathway transcripts⁴ (Extended Data Fig. 6). To follow-up on possible metabolic differences between parasites persisting through

the dry season and parasites causing malaria in the transmission season, we used liquid chromatography–mass spectrometry (LC–MS) to profile both hydrophilic and hydrophobic metabolites from the plasma of 12 subclinical children with *P. falciparum* infections at the end of the dry season (May) and of 12 children presenting with their first clinical malaria case (MAL) in the rainy season. We



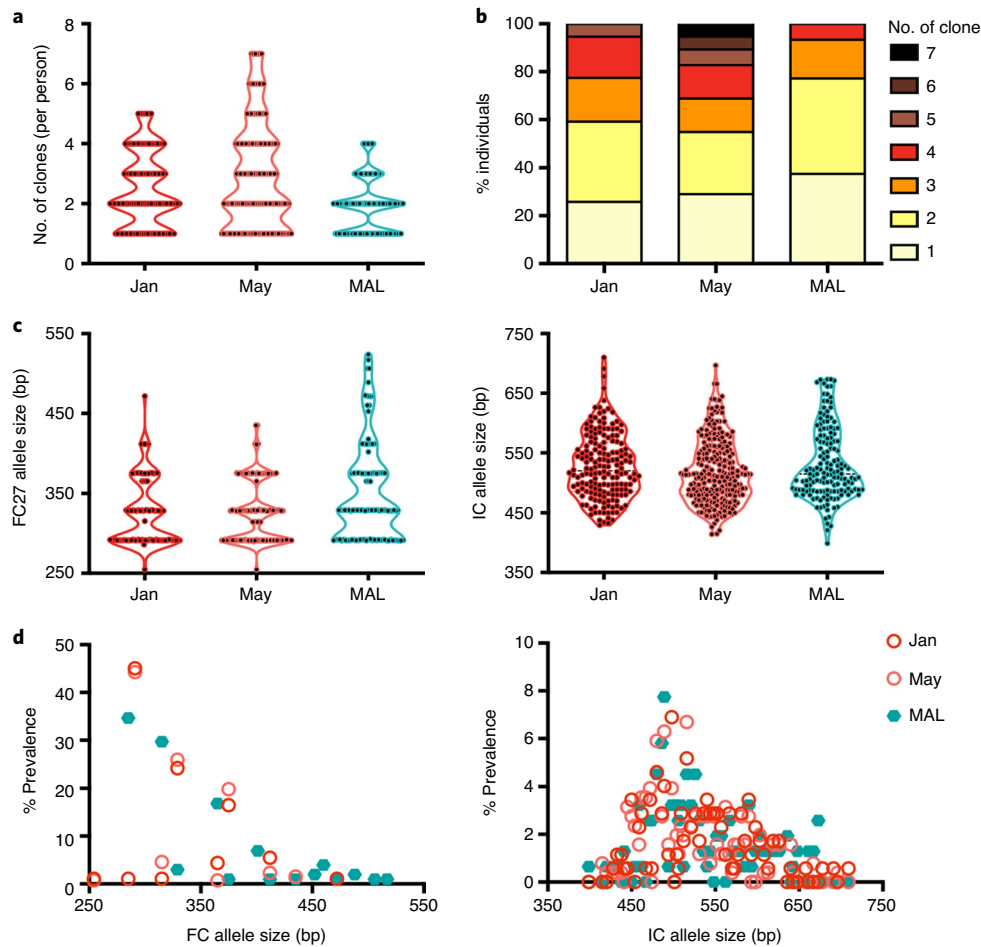


Fig. 3 | *P. falciparum* genetic diversity is maintained throughout the year. **a**, Number of *P. falciparum* clones in subclinical PCR⁺ children in beginning (Jan) and end (May) of the dry season, and first clinical malaria case (MAL) during the transmission season, determined by differences in size of a polymorphic region of *msp2*. **b**, Proportion of individuals with different numbers of *P. falciparum* clones in the beginning (January) and end (May) of the dry season and clinical malaria cases (MAL). **c**, Size of the *msp2* alleles FC27 (left) and IC/3D7 (right) in the beginning (January) and end (May) of the dry season and clinical malaria cases (MAL). **d**, Prevalence of *msp2* clone sizes of FC27 (left) and IC/3D7 (right) allelic families in January ($n=93$), May ($n=93$) and clinical malaria (MAL, $n=136$). All violin plots show all data points; Mood's median test.

found significant separation between metabolites present in the two groups of samples (Fig. 4h and Supplementary Table 8); however, the difficulty of normalization of measured metabolite levels to parasite burden, plus the strong parasitemia differences at the time of the blood draw, hinder conclusive interpretation of what might be seasonal or parasite-induced metabolic alterations (Supplementary Table 9).

***P. falciparum* replication is not impaired in the dry season.** We then tested the hypothesis that dry season parasitemias were maintained low and subclinical due to decreased parasite replication capacity during this period. We cultured *P. falciparum* for 36–48 h in vitro directly after blood draw from rapid diagnostic test positive (RDT⁺) samples of asymptomatic individuals at three time points of the dry season (January, March and May) and from samples of children presenting with their first clinical malaria episode of the ensuing transmission season (MAL). By flow cytometry, we measured the increase in parasitemia and parasite development at 0, 16, 24, 30, 36 and 48 h after in vitro culture. Parasite in vitro growth rates of samples from more than 40 subclinical donors during the dry season and ~30 malaria cases in the transmission season indicated that the highest growth determined between any two time points of the short-term culture was similar throughout the year. During

the 36- to 48-h in vitro culture, parasitemias increased between two- and fivefold at any point in the year: 2.8-fold in January, 95% CI (2.3, 3.3); 4.1-fold in March, 95% CI (3.4, 4.7); 3.6-fold in May, 95% CI (2.6, 4.6); and 2.8-fold in malaria cases, 95% CI (2.1, 3.5). However, the number of hours in culture needed to increase parasitemia was shorter in the dry season samples than in samples from malaria-causing parasites in the transmission season (Fig. 5a). In accordance with an earlier increase in parasitemia in vitro during the dry season, we could frequently identify on Giemsa smears mature schizonts after 16 and 24 h of culture and young ring stages after 30 or 36 h in the dry season samples, whereas mature schizonts of malaria-causing parasite samples were mostly observed after 36 h in culture, and young ring stages were largely found after 48 h in vitro (Fig. 5b). When we calculated the number of hours in culture at which the highest increase of parasitemia could be detected for each sample, we observed that it decreased from the beginning to the end of the dry season—January, 26.4 h, 95% CI (24.5, 28.3); March, 24.9 h, 95% CI (23.9, 25.9); May, 22.7 h, 95% CI (20.8, 24.6)—and was maximal during malaria cases in the transmission season, MAL 44.0 h, 95% CI (41.5, 46.6) (Fig. 5c). Nevertheless, when we measured the number of merozoites per multinucleated schizont before or at the time of the highest increase in parasitemia in vitro, we obtained similar values at the end of dry season and in clinical malaria cases

in the wet season (Fig. 5d). Finding later developmental parasite stages at earlier times in this short-term *in vitro* experiment during the dry season could indicate a faster than 48-h intraerythrocytic replicative cycle, or, alternatively, that dry season parasites circulate longer without adhering to the host vascular endothelium and were more developed than circulating parasites in clinical malaria cases at the time of the blood draw. To test the latter, we used the RNA-seq data described in Fig. 4 to estimate, with a likelihood-based statistical method previously described²⁸, the age in hours post-invasion (hpi) of circulating parasites from subclinical children at the end of the dry season (May) and from clinical cases during the wet season (MAL). We determined that parasites circulating in the dry season had a transcriptional signature of ~17 hpi, 95%CI (14.05, 20.8), whereas parasites circulating in malaria cases during the wet season had a transcription profile similar to parasites with ~7 hpi, 95% CI (6.5, 7.7) (Fig. 5e). Accordingly, imaging the thick blood films made in the field at the time of the blood draw, we confirmed that the more developed trophozoite stages of *P. falciparum* were present on subclinical samples collected at the end dry season, whereas clinical malaria samples in the transmission season presented much smaller ring stages of *P. falciparum* (Fig. 5f,g). All together, these data show that, at the end of the dry season, *P. falciparum* can be found circulating at later stages of the ~48-h asexual cycle than what is seen during clinical malaria cases in the wet season.

Infected erythrocytes in circulation at the end of the dry season are at higher risk of splenic clearance. To investigate if longer circulation of iRBCs in the dry season would affect host RBC deformability and potentiate splenic clearance, we used a microfiltration system mimicking the narrow and short inter-endothelial slits of the human spleen with different-sized microspheres²⁹. Using freshly collected blood samples from asymptotically infected children at the end of the dry season and from children presenting with febrile malaria during the transmission season, we assessed retention in the microspheres and flow-through of circulating iRBCs at time 0 and after 6, 18 and 30 h *in vitro*. We observed that iRBCs collected from malaria (MAL) cases were not significantly retained in the spleen-like system at 0, 6 or 18 h after culture and that only after 30 h was the percentage of iRBCs in the flow-through reduced, indicating splenic retention of iRBCs (Fig. 6a). Conversely, iRBCs in RDT⁺ blood collected at the end of the dry season (May) had significantly reduced flow-through immediately after the blood draw (~25% retention of 0-h iRBCs in the microsphere system) and over 50% retention of iRBCs after 6 or 18 h in culture (Fig. 6a). Accordingly, we observed that trophozoites or schizonts that fail to flow through the microsphere system were circulating (at 0 h) only in the dry season samples (Fig. 6b).

We then investigated whether differences in cyto-adhesion, affecting the length of time that parasitized cells remain in circulation, could explain the observed parasite age distributions and microfiltration results. For this, we used a mathematical model to describe the within-host growth and removal of iRBCs from circulation through cyto-adhesion in the vasculature and through

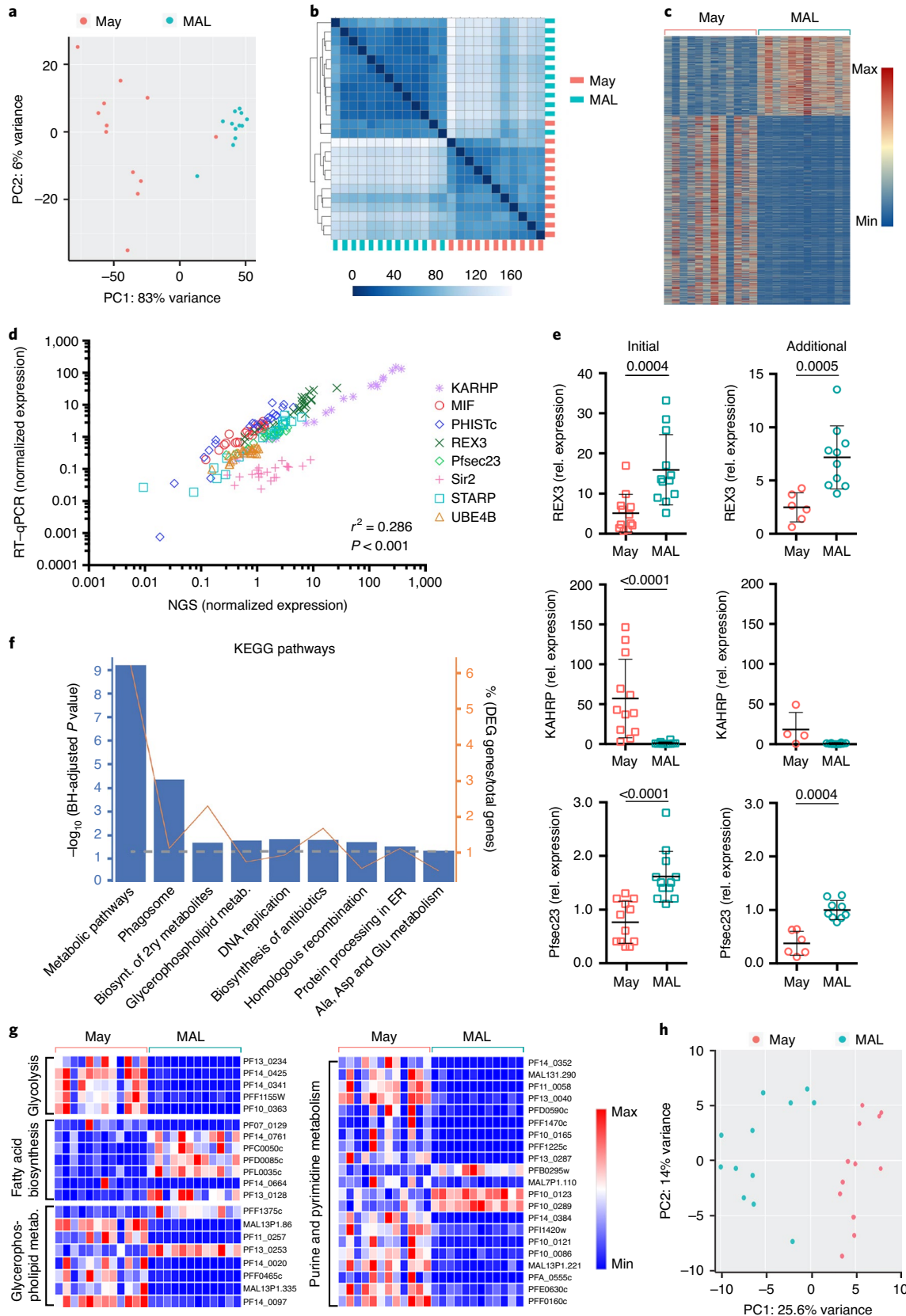
splenic retention (Methods). Both processes were assumed to be dependent on the parasite's developmental stage, increasing as the parasite starts to express adherence-mediating surface antigens, and RBC modification leads to cell rigidity. Whereas cyto-adhering parasites still replicate, those filtered out by the spleen were assumed to be removed. As shown in Fig. 6c, effective growth rates and population sizes of low-cyto-adhering parasites are significantly lower than those of high-cyto-adhering parasites, which can avoid splenic clearance before parasitized cells become too rigid to pass through the spleen. We then obtained estimated parasite age distributions for both scenarios (Fig. 6d) by sampling from the modeled parasite population at random points over the simulated infection time course, akin to blood sampling from a population. As low-adhesion parasites are predominantly removed by the spleen toward the end of their life cycle, they show a much broader age range than high-cyto-adhesion parasites, which are removed from circulation earlier through cyto-adhesion and, therefore, show a narrower and younger age range, in agreement with the observed age distribution from thick blood smears (Fig. 5e,f). Next, we simulated a microfiltration experiment by 'growing' our sampled model parasites older and evaluating their projected average flow-through based on our assumed, age-dependent splenic retention function (Methods and Extended Data Fig. 7). The throughput of high-cyto-adhering parasites is high for the first 6–10 h before dropping off gradually as parasites grow older (Fig. 6e). In contrast, samples from low-cyto-adhering parasites, with their more uniformly distributed age range, already have a much reduced flow-through at 0 h, which, however, remained more stable as parasites mature over the next 30 h—again, in line with the empirical observations (Fig. 6a). These mathematical results suggest that cyto-adhesion alone can explain the differences between parasites sampled during the dry season (low-adhesion) and parasites sampled from malaria cases (high-adhesion).

To investigate whether the expression of cyto-adhesion-mediating PfEMP1 proteins differed in abundance or quality in subclinical parasites from the dry season compared to parasites found in malaria cases during the wet season, we assembled the *var* genes from the RNA-seq reads of the 24 samples from the end of the dry season and the malaria cases (Methods). Expression of several *var* genes has been shown to remain fairly stable between ~10 and 20 h after invasion³⁰, which should be close to the average ages estimated for parasites in malaria cases and dry season samples, respectively. Using a recently developed analytical pipeline³¹, we could detect LARSFADIG motifs identifying PfEMP1 coding genes³² in eight of 12 samples from the dry season and in ten of 12 malaria cases (Extended Data Fig. 8). We were able to annotate full-length *var* genes, including both the start N-terminal sequence (NTS) and the acidic terminal sequence (ATS) domains, and also many isolated fragments, and we observed more contigs with LARSFADIG motifs and *var* gene fragments in the wet season samples (Supplementary Table 10). We used different methods to access enrichment of higher expressed *var* genes in the wet versus the dry season samples. Although we did not see statistically significant enrichment,

Fig. 4 | Transcriptome of circulating *P. falciparum* at the end of the dry season differs from malaria-causing *P. falciparum* during the transmission season. **a,b** Principal component (a) and unsupervised clustering (b) analyses of RNA-seq data of *P. falciparum* parasites collected at the end of the dry season and from clinical malaria cases ($n=12$ May, 12 MAL). **c**, Heat map showing normalized reads of DEGs (rows) for each individual (columns) from *P. falciparum* collected at the end of the dry season (May) and at the first clinical malaria case (MAL) in the ensuing transmission season. **d**, RT-qPCR validation of RNA-seq data for eight labeled DEGs ($n=24$). P and r^2 determined by Pearson's correlation. **e**, RT-qPCR validation of initial 24 RNA-seq samples (left) and 18 additional samples (right) for three DEGs. Data indicate mean \pm s.d.; two-tailed Mann-Whitney test. **f**, Summary of KEGG pathways significantly enriched with DEGs. Blue bars indicate P_{adj} for enrichment of each pathway. The gray dashed line indicates the threshold $P=0.05$; the orange line indicates the percentage of genes in each pathway present in the DEG list. **g**, Heat map showing normalized reads of DEGs involved in different metabolic pathways (rows) for each individual (columns) from *P. falciparum* at the end of the dry season and at the first clinical malaria case ($n=12$ May, 12 MAL). **h**, Principal component analysis of target metabolite data of plasmas from subclinical *P. falciparum* carriers at the end of the dry season and from clinical malaria cases ($n=12$ May, 12 MAL).

we observed a trend that the top expressed *var* genes in each individual in the wet season are more highly expressed (Fig. 6f), and we plan further studies with larger samples size to verify this

trend. Furthermore, we identified known *var* gene domains such as Duffy binding-like (DBL) and cysteine-rich interdomain region (CIDR), as well as the NTS and ATS, and searched for typical 5'



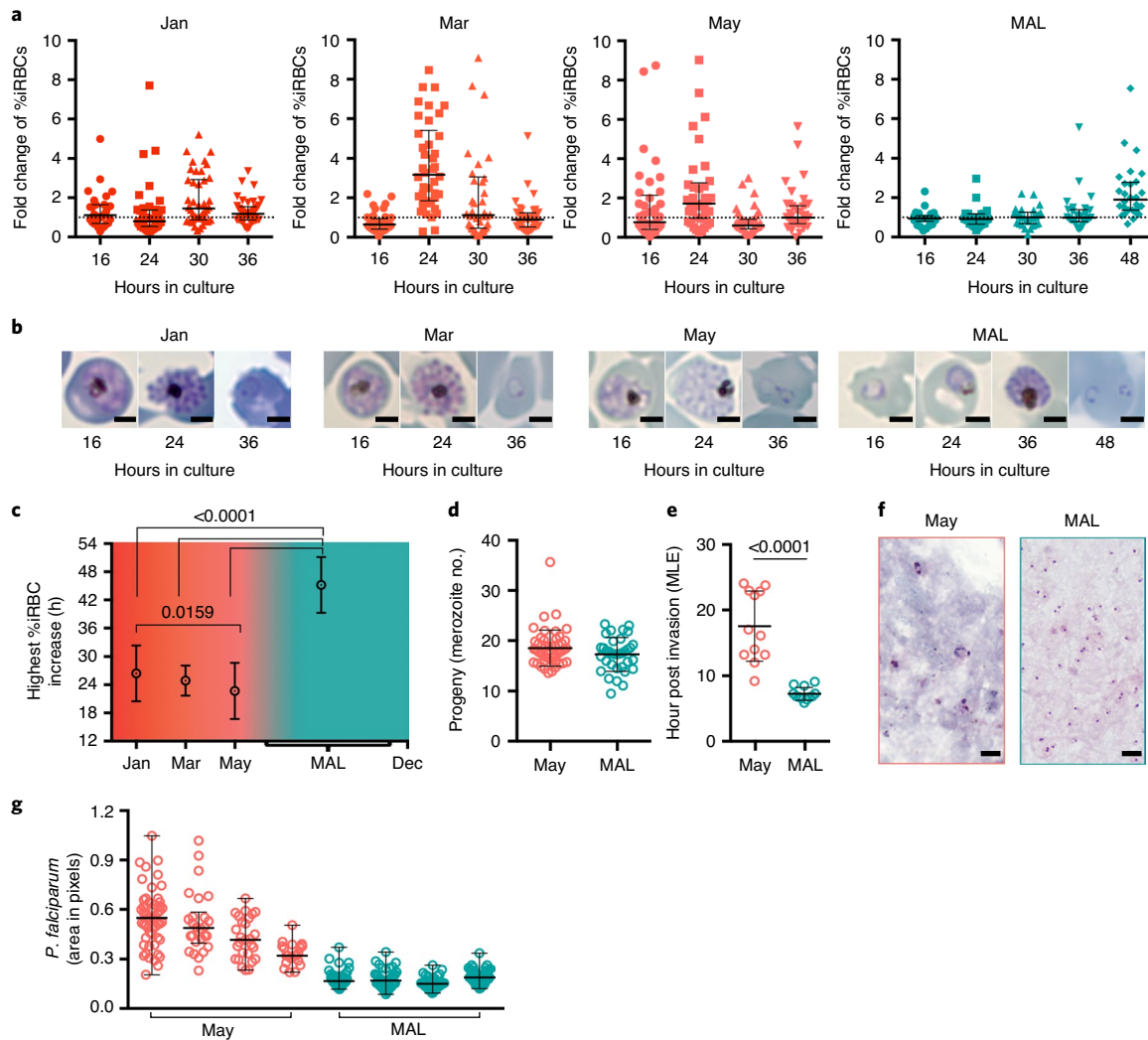


Fig. 5 | Replication of persistent dry season *P. falciparum* is not impaired. **a**, Parasitemia fold change at 16, 24, 30, 36 and 48 h after culture of parasites collected from children at different times during the dry season (January, March and May) and clinical malaria cases (MAL). Fold change is defined as %iRBC t(n)/%iRBC t(n-1). Data indicate median \pm IQR. Dashed line at fold change of 1. One-sided Dunn's Kruskal-Wallis multiple comparisons test. **b**, Giemsa-stained thin blood smears 16, 24, 36 or 48 h after culture of *P. falciparum* parasites collected from children during the dry season (January, March and May) and clinical malaria cases (MAL). Scale bar, 2 μ m. **c**, Time of highest increase in parasitemia detected during in vitro culture of *P. falciparum* parasites from children in January ($n=39$), March ($n=42$) and May ($n=40$) during the dry season, and clinical malaria cases (MAL, $n=27$). Data indicate mean \pm s.d.; one-sided Dunn's Kruskal-Wallis multiple comparisons test. **d**, Number of merozoites inside multinucleated schizonts determined by flow cytometry at the end of the dry season (May, $n=50$) and clinical malaria (MAL, $n=35$) samples. Data indicate mean \pm s.d.; two-tailed Mann-Whitney test. **e**, Maximum likelihood estimation (MLE) of the hpi of dry season (May, $n=12$) and clinical malaria (MAL, $n=12$) parasites. Data indicate mean \pm s.d.; two-tailed Mann-Whitney test. **f**, Giemsa-stained thick blood films of *P. falciparum* parasites collected straight from the arms of children at the end of the dry season (May) and at their first clinical malaria (MAL). Scale bar, 5 μ m. **g**, *P. falciparum* area measured from Giemsa-stained thick smears in subclinical infections at the end of the dry season (May) and in malaria cases (MAL) in the wet season. Data indicate median \pm IQR; two-tailed Mann-Whitney test, $P < 0.0001$. IQR, interquartile range.

UPS sequences associating with different pathological outcomes²² in the dry season and malaria case assembled *vars*. Although we were unable to determine the UPS type of expressed *vars* owing to the short assembly of the 5' UTR region, we did find more *var* genes with a DBLz domain in the malaria samples (13 of 61 in *var* fragments longer than 3.5 kb) compared to the dry season (one of 11 in *var* fragments longer than 3.5 kb) (Supplementary Table 10).

Discussion

Asymptomatic individuals carrying *P. falciparum* at the end of the dry season in areas of seasonal malaria have been broadly described^{13,33–37}, but how the parasite bridges two rainy seasons

without promoting malaria symptoms or being cleared remained elusive. In this study, with samples from Malians exposed to alternating 6-month dry and transmission seasons, we show that, within each 48-h replicative cycle, *P. falciparum* iRBCs circulate longer in the bloodstream during the dry season, allowing increased clearance in the spleen and thus preventing high parasitemias, which could lead to immune activation or malaria symptoms^{38,39}.

Although asymptomatic parasitemia at the end of the dry season associates with a lower risk of clinical malaria in the ensuing wet season^{13,33–35}, clearance of parasitemia with anti-malarials before the transmission season does not increase subsequent malaria risk, and the persistence of infection during the dry season does not prevent

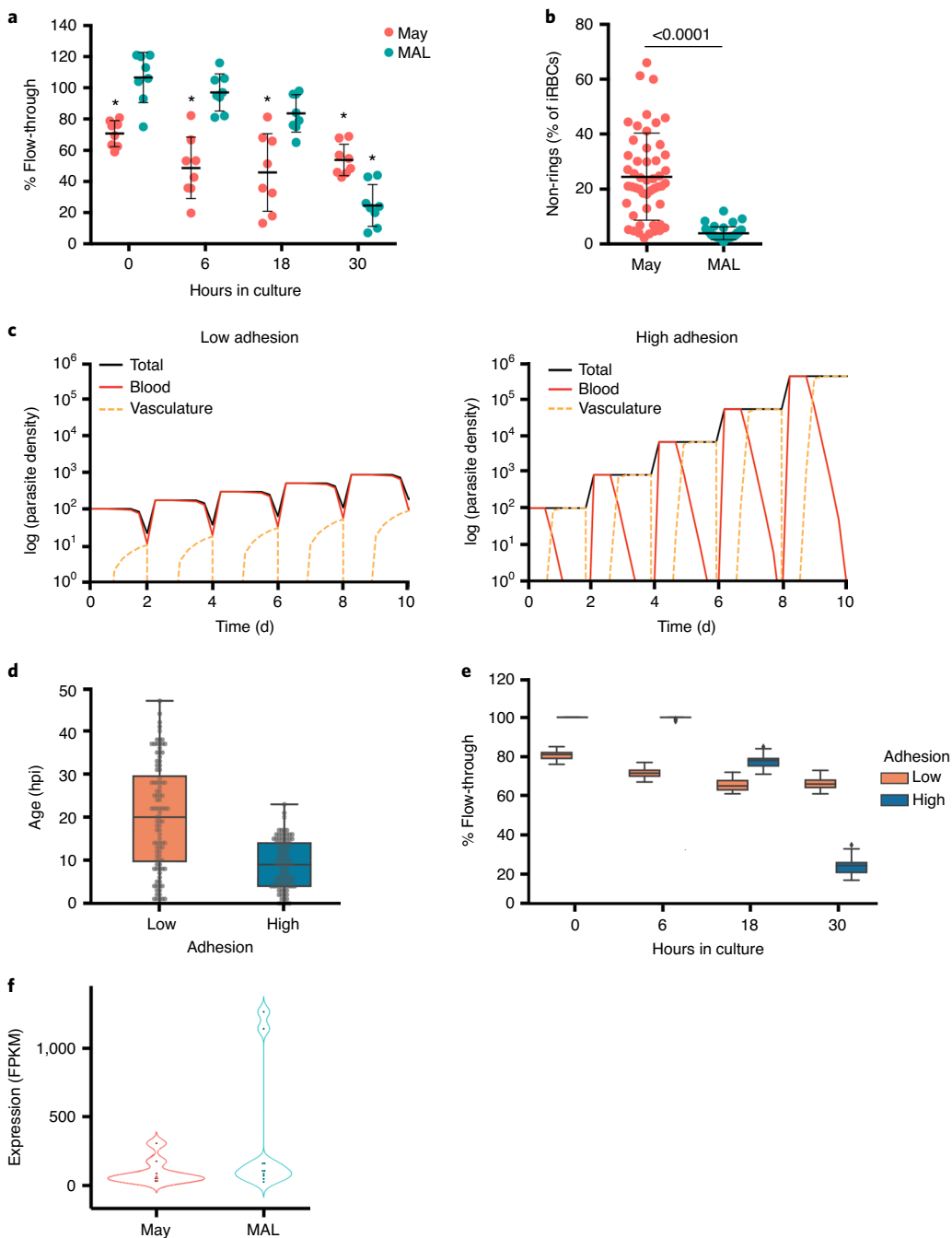


Fig. 6 | Infected erythrocytes in circulation at the end of the dry season are at higher risk of splenic clearance. **a**, *P. falciparum* iRBC filtration through beads mimicking the human spleen at 0, 6, 18 and 30 h after culture at the end of the dry season and during clinical malaria ($n=8$ May, 8 MAL) relative to the non-filtered same-time control. Flow-through percentage is defined as $(\text{downstream \%iRBCs}/\text{upstream \%iRBCs}) \times 100$. Data indicate mean \pm s.d.; one-sided Dunn's Kruskal-Wallis multiple comparisons test of the mean rank of each condition to 0-h MAL; * shows $P < 0.001$. **b**, Percentage of circulating non-ring stage iRBCs at the end of the dry season and during malaria cases ($n=50$ May, 39 MAL) determined by flow cytometry. Mean \pm s.d.; two-tailed Mann-Whitney test. **c**, Within-host dynamics simulation of growth rates and population sizes over five replication cycles of low-cyto-adhering (left) and high-cyto-adhering (right) parasites, stratified as circulating (red lines), cyto-adhering (orange dashed lines) and total biomass (black lines). **d**, Simulation of circulating parasite age distribution over two replication cycles after repeated sampling of low-cyto-adhering parasites (Low, $n=100$) and high-cyto-adhering parasites (High, $n=100$). **e**, Simulation of circulation and passage through the spleen of independently sampled parasites aging over time, with low-cyto-adhering (Low, $n=50$) and high-cyto-adhering (High, $n=50$) parasites. **f**, Expression level of the highest expressed *var* gene at the end of the dry season and during a clinical malaria case ($n=8$ May, 10 MAL). Box plots (**d**, **e**) indicate the median \pm IQR and the minimum ($Q1 - 1.5 \times IQR$) and maximum ($Q3 + 1.5 \times IQR$) of the data range (whiskers). IQR, interquartile range.

or slow the decline of *P. falciparum*-specific antibodies¹³ (Fig. 2f,g). Consistent with these observations, low parasitemia during the dry season did not elicit detectable inflammation or affect immune cell

function (Fig. 2), indicating that chronic low parasitemia in seasonal endemic settings might differ from controlled human malaria infections (CHMIs) in naive individuals, where low parasitemias

appear to induce immunity⁴⁰, and also suggesting that slow and continuous stimulation of the immune system is less effective than sudden changes in antigenic stimulation⁴¹. Nevertheless, cumulative immunity might be required to sustain the dry season reservoir of *P. falciparum*. Dry season subclinical carriers have higher anti-*P. falciparum* humoral immunity (ref. ¹³ and Fig. 2f,g) and higher *P. falciparum*-specific MBCs (Fig. 2e) than non-infected individuals, suggesting that a certain level of cumulative exposure is necessary to carry dry season subclinical infections. Additionally, we and others have shown that end-of-dry-season parasitemias are more frequent in older than younger children^{13,42}, which is consistent with an age-dependent decrease in parasitemia and increase in anti-parasitic immunity^{43,44}. It is possible that, within each *P. falciparum* infection, sequential presentation of different VSAs on the surface of iRBCs and its corresponding ordered acquisition of antibodies^{45,46} favor progressively less virulent parasites. Accordingly, a recent study of CHMI, including naive and semi-immune individuals, observed clinical cases in naive individuals, whereas chronic infections appeared in semi-immune individuals with intermediate antibody levels⁴⁷.

Reports from the transmission season show that increasing malaria severity associates with different parasite transcriptional profiles^{26,48–50}, but the persisting dry season reservoir had not been investigated. Our data show that, whereas *P. falciparum*-causing malaria in the transmission season has a ring stage transcriptional signature, parasites persisting at the end of the dry season resemble more developed intraerythrocytic stages, which we confirmed both visually and through differential growth kinetics in vitro (Fig. 5). Future single-cell transcript analysis of iRBCs⁵ will allow comparing stage-matched pools of parasites to better understand how *P. falciparum* achieves low cyto-adhesion in the dry season. Also of interest will be to revisit earlier reports of transcriptional differences between parasites, inducing varying degrees of malaria severity^{26,48,49}, and to question whether these could be partially imposed by the hpi of circulating parasites. In fact, Tonkin-Hill and colleagues found a bias toward early trophozoite transcription in non-severe malaria samples compared to the ring stage transcriptional profile of severe malaria cases⁴⁸, which could be due to differing adhesion efficiencies in vivo. Interestingly, in vitro replication rates of severe and uncomplicated malaria-causing parasites^{51,52} have not consistently explained the higher parasitemias observed in severe malaria cases, suggesting that adhesion efficiency differences might also contribute. Continued asexual replication (independently or coupled with immunity) might lead to progressively less adhesive iRBCs, as observed in parasites collected during the dry season. In a rodent-malaria model, uninterrupted asexual-stage growth led to bias in gene expression of VSA and parasite virulence⁵³, and the transition between acute and chronic phases is suggested to be independent of adaptive immunity⁵⁴. Also, in humans, it has been suggested that continued asexual replication can skew the PfEMP1 expression profile^{47,55}, which is consistent with our var genes RNA-seq data (Fig. 6f and Extended Data Fig. 8). The mechanisms by which the parasite adapts to the dry season, and how transmission is assured as the rainy season ensues, remain to be investigated. In a varying or unpredictable environment, organisms can overcome unfavorable conditions by sensing environmental changes and adapting their individual developmental program to increase survival. Alternatively, stochastic population heterogeneity can increase the probability of survival under changing conditions⁵⁶. *P. falciparum* might sense and respond to environmental cues of transmissibility opportunity, as has been described for detection of nutrient availability⁵⁷, sexual commitment⁵⁸ or appropriate environment for gametogenesis⁵⁹. Such a mechanism could act through epigenetic modulation of VSAs, or be seasonally imposed by different metabolic states of the host, driving a shift of the parasite from a fast- to a slow-growing program as the transmission season ends

and persistence is required, and returning to fast growth as transmission resumes. In an avian-malaria model, chronic *Plasmodium relictum* was shown to respond to bites from uninfected mosquitoes and increase its replication, promoting transmission⁶⁰. Parasite survival during the dry season is imperative but will be efficient in resuming transmission only if these retain the ability to produce gametocytes that mosquitoes can uptake. Thus, investigating potential adaptive changes in the sexual stages of *P. falciparum* during the dry season will likely also reveal seasonal adjustments. Investigating the transcriptional profile of the few malaria cases diagnosed in the dry season (Fig. 1a and Extended Data Fig. 2) should be the focus of future studies.

In conclusion, the survival of *P. falciparum*-infected individuals during the dry season is advantageous for the parasite, and low adhesion of infected erythrocytes is likely a central feature to the subclinical carriage of *P. falciparum*, demonstrating the adaptability of *P. falciparum* parasites to the vector-free period.

Online content

Any methods, additional references, Nature Research reporting summaries, source data, extended data, supplementary information, acknowledgements, peer review information; details of author contributions and competing interests; and statements of data and code availability are available at <https://doi.org/10.1038/s41591-020-1084-0>.

Received: 2 April 2020; Accepted: 27 August 2020;

Published online: 26 October 2020

References

1. World Health Organization. *World malaria report 2019* <https://www.who.int/malaria/publications/world-malaria-report-2019/en/> (2019).
2. Hommel, M., David, P. H. & Oligino, L. D. Surface alterations of erythrocytes in *Plasmodium falciparum* malaria. Antigenic variation, antigenic diversity, and the role of the spleen. *J. Exp. Med.* **157**, 1137–1148 (1983).
3. Roberts, D. J. et al. Rapid switching to multiple antigenic and adhesive phenotypes in malaria. *Nature* **357**, 689–692 (1992).
4. Bozdech, Z. et al. The transcriptome of the intraerythrocytic developmental cycle of *Plasmodium falciparum*. *PLoS Biol.* **1**, E5 (2003).
5. Howick, V. M. et al. The Malaria Cell Atlas: single parasite transcriptomes across the complete *Plasmodium* life cycle. *Science* **365**, eaaw2619 (2019).
6. Marti, M., Good, R. T., Rug, M., Kneuper, E. & Cowman, A. F. Targeting malaria virulence and remodeling proteins to the host erythrocyte. *Science* **306**, 1930–1933 (2004).
7. Crabb, B. S. et al. Targeted gene disruption shows that knobs enable malaria-infected red cells to cytoadhere under physiological shear stress. *Cell* **89**, 287–296 (1997).
8. Oh, S. S. et al. *Plasmodium falciparum* erythrocyte membrane protein 1 is anchored to the actin-spectrin junction and knob-associated histidine-rich protein in the erythrocyte skeleton. *Mol. Biochem. Parasitol.* **108**, 237–247 (2000).
9. Lavstsen, T. et al. *Plasmodium falciparum* erythrocyte membrane protein 1 domain cassettes 8 and 13 are associated with severe malaria in children. *Proc. Natl Acad. Sci. USA* **109**, E1791–E1800 (2012).
10. Lehmann, T. et al. Aestivation of the African malaria mosquito, *Anopheles gambiae* in the Sahel. *Am. J. Trop. Med. Hyg.* **83**, 601–606 (2010).
11. Babiker, H. A., Abdel-Muhsin, A. M., Ranford-Cartwright, L. C., Satti, G. & Walliker, D. Characteristics of *Plasmodium falciparum* parasites that survive the lengthy dry season in eastern Sudan where malaria transmission is markedly seasonal. *Am. J. Trop. Med. Hyg.* **59**, 582–590 (1998).
12. Ouedraogo, A. L. et al. Dynamics of the human infectious reservoir for malaria determined by mosquito feeding assays and ultrasensitive malaria diagnosis in Burkina Faso. *J. Infect. Dis.* **213**, 90–99 (2016).
13. Portugal, S. et al. Treatment of chronic asymptomatic *Plasmodium falciparum* infection does not increase the risk of clinical malaria upon reinfection. *Clin. Infect. Dis.* **64**, 645–653 (2017).
14. Kimenyi, K. M., Wamae, K. & Ochola-Oyier, L. I. Understanding *P. falciparum* asymptomatic infections: a proposition for a transcriptomic approach. *Front. Immunol.* **10**, 2398 (2019).
15. O'Donnell, A. et al. The acute phase response in children with mild and severe malaria in Papua New Guinea. *Trans. R. Soc. Trop. Med. Hyg.* **103**, 679–686 (2009).

16. Park, G. S., Ireland, K. F., Opoka, R. O. & John, C. C. Evidence of endothelial activation in asymptomatic *Plasmodium falciparum* parasitemia and effect of blood group on levels of von Willebrand factor in malaria. *J. Pediatr. Infect. Dis. Soc.* **1**, 16–25 (2012).
17. Burte, F. et al. Circulatory hepcidin is associated with the anti-inflammatory response but not with iron or anemic status in childhood malaria. *Blood* **121**, 3016–3022 (2013).
18. Weinberg, J. B. et al. Monocyte polarization in children with *falciparum* malaria: relationship to nitric oxide insufficiency and disease severity. *Sci. Rep.* **6**, 29151 (2016).
19. Oyegue-Liabagu, S. L. et al. Pro- and anti-inflammatory cytokines in children with malaria in Franceville, Gabon. *Am. J. Clin. Exp. Immunol.* **6**, 9–20 (2017).
20. Lyke, K. E. et al. Serum levels of the proinflammatory cytokines interleukin-1 β (IL-1 β), IL-6, IL-8, IL-10, tumor necrosis factor α , and IL-12(p70) in Malian children with severe *Plasmodium falciparum* malaria and matched uncomplicated malaria or healthy controls. *Infect. Immun.* **72**, 5630–5637 (2004).
21. Hopp, C. S. et al. *Plasmodium falciparum*-specific IgM B cells dominate in children, expand with malaria and produce parasite inhibitory IgM. Preprint at <https://www.biorxiv.org/content/10.1101/2020.04.12.030049v2> (2020).
22. Lavstsen, T., Salanti, A., Jensen, A. T., Arnot, D. E. & Theander, T. G. Sub-grouping of *Plasmodium falciparum* 3D7 var genes based on sequence analysis of coding and non-coding regions. *Malar. J.* **2**, 27 (2003).
23. Cowman, A. F., Berry, D. & Baum, J. The cellular and molecular basis for malaria parasite invasion of the human red blood cell. *J. Cell Biol.* **198**, 961–971 (2012).
24. Snounou, G. et al. Biased distribution of msp1 and msp2 allelic variants in *Plasmodium falciparum* populations in Thailand. *Trans. R. Soc. Trop. Med. Hyg.* **93**, 369–374 (1999).
25. Liljander, A. et al. Optimization and validation of multi-coloured capillary electrophoresis for genotyping of *Plasmodium falciparum* merozoite surface proteins (msp1 and 2). *Malar. J.* **8**, 78 (2009).
26. Daily, J. P. et al. Distinct physiological states of *Plasmodium falciparum* in malaria-infected patients. *Nature* **450**, 1091–1095 (2007).
27. Rono, M. K. et al. Adaptation of *Plasmodium falciparum* to its transmission environment. *Nat. Ecol. Evol.* **2**, 377–387 (2018).
28. Lemieux, J. E. et al. Statistical estimation of cell-cycle progression and lineage commitment in *Plasmodium falciparum* reveals a homogeneous pattern of transcription in ex vivo culture. *Proc. Natl Acad. Sci. USA* **106**, 7559–7564 (2009).
29. Deplaine, G. et al. The sensing of poorly deformable red blood cells by the human spleen can be mimicked in vitro. *Blood* **117**, e88–e95 (2011).
30. Dahlback, M. et al. Changes in var gene mRNA levels during erythrocytic development in two phenotypically distinct *Plasmodium falciparum* parasites. *Malar. J.* **6**, 78 (2007).
31. Otto, T. D. et al. Evolutionary analysis of the most polymorphic gene family in *falciparum* malaria. *Wellcome Open Res.* **4**, 193 (2019).
32. Otto, T. D. et al. Genome sequencing of chimpanzee malaria parasites reveals possible pathways of adaptation to human hosts. *Nat. Commun.* **5**, 4754 (2014).
33. Sonden, K. et al. Asymptomatic multiclonal *Plasmodium falciparum* infections carried through the dry season predict protection against subsequent clinical malaria. *J. Infect. Dis.* **212**, 608–616 (2015).
34. Males, S., Gaye, O. & Garcia, A. Long-term asymptomatic carriage of *Plasmodium falciparum* protects from malaria attacks: a prospective study among Senegalese children. *Clin. Infect. Dis.* **46**, 516–522 (2008).
35. Crompton, P. D. et al. Sickle cell trait is associated with a delayed onset of malaria: implications for time-to-event analysis in clinical studies of malaria. *J. Infect. Dis.* **198**, 1265–1275 (2008).
36. Drakeley, C., Sutherland, C., Bousema, J. T., Sauerwein, R. W. & Targett, G. A. The epidemiology of *Plasmodium falciparum* gametocytes: weapons of mass dispersion. *Trends Parasitol.* **22**, 424–430 (2006).
37. Bousema, T. et al. Mosquito feeding assays to determine the infectiousness of naturally infected *Plasmodium falciparum* gametocyte carriers. *PLoS ONE* **7**, e42821 (2012).
38. Dicko, A. et al. Season, fever prevalence and pyrogenic threshold for malaria disease definition in an endemic area of Mali. *Trop. Med. Int. Health* **10**, 550–556 (2005).
39. Smith, T., Schellenberg, J. A. & Hayes, R. Attributable fraction estimates and case definitions for malaria in endemic areas. *Stat. Med.* **13**, 2345–2358 (1994).
40. Stanisic, D. I., McCarthy, J. S. & Good, M. F. Controlled human malaria infection: applications, advances, and challenges. *Infect. Immun.* **86**, e00479-17 (2018).
41. Pradeu, T. & Vivier, E. The discontinuity theory of immunity. *Sci. Immunol.* **1**, AAG0479 (2016).
42. Goncalves, B. P. et al. Examining the human infectious reservoir for *Plasmodium falciparum* malaria in areas of differing transmission intensity. *Nat. Commun.* **8**, 1133 (2017).
43. Tran, T. M. et al. An intensive longitudinal cohort study of Malian children and adults reveals no evidence of acquired immunity to *Plasmodium falciparum* infection. *Clin. Infect. Dis.* **57**, 40–47 (2013).
44. Crompton, P. D. et al. A prospective analysis of the Ab response to *Plasmodium falciparum* before and after a malaria season by protein microarray. *Proc. Natl Acad. Sci. USA* **107**, 6958–6963 (2010).
45. Cham, G. K. et al. Hierarchical, domain type-specific acquisition of antibodies to *Plasmodium falciparum* erythrocyte membrane protein 1 in Tanzanian children. *Infect. Immun.* **78**, 4653–4659 (2010).
46. Obeng-Adjei, N. et al. Longitudinal analysis of naturally acquired PfEMP1 CIDR domain variant antibodies identifies associations with malaria protection. *JCI Insight* **5**, e167232 (2020).
47. Bachmann, A. et al. Controlled human malaria infection with *Plasmodium falciparum* demonstrates impact of naturally acquired immunity on virulence gene expression. *PLoS Pathog.* **15**, e1007906 (2019).
48. Tonkin-Hill, G. Q. et al. The *Plasmodium falciparum* transcriptome in severe malaria reveals altered expression of genes involved in important processes including surface antigen-encoding var genes. *PLoS Biol.* **16**, e2004328 (2018).
49. Almelli, T. et al. Differences in gene transcriptomic pattern of *Plasmodium falciparum* in children with cerebral malaria and asymptomatic carriers. *PLoS ONE* **9**, e114401 (2014).
50. Lee, H. J. et al. Integrated pathogen load and dual transcriptome analysis of systemic host-pathogen interactions in severe malaria. *Sci. Transl. Med.* **10**, eaar3619 (2018).
51. Deans, A. M. et al. Low multiplication rates of African *Plasmodium falciparum* isolates and lack of association of multiplication rate and red blood cell selectivity with malaria virulence. *Am. J. Trop. Med. Hyg.* **74**, 554–563 (2006).
52. Chotivanich, K. et al. Parasite multiplication potential and the severity of *falciparum* malaria. *J. Infect. Dis.* **181**, 1206–1209 (2000).
53. Spence, P. J. et al. Vector transmission regulates immune control of *Plasmodium* virulence. *Nature* **498**, 228–231 (2013).
54. Brugat, T. et al. Antibody-independent mechanisms regulate the establishment of chronic *Plasmodium* infection. *Nat. Microbiol.* **2**, 16276 (2017).
55. Abdi, A. I. et al. Global selection of *Plasmodium falciparum* virulence antigen expression by host antibodies. *Sci. Rep.* **6**, 19882 (2016).
56. Weinberger, L. S. A minimal fate-selection switch. *Curr. Opin. Cell Biol.* **37**, 111–118 (2015).
57. Mancio-Silva, L. et al. Nutrient sensing modulates malaria parasite virulence. *Nature* **547**, 213–216 (2017).
58. Brancucci, N. M. B. et al. Lysophosphatidylcholine regulates sexual stage differentiation in the human malaria parasite *Plasmodium falciparum*. *Cell* **171**, 1532–1544 (2017).
59. Billker, O. et al. Identification of xanthurenic acid as the putative inducer of malaria development in the mosquito. *Nature* **392**, 289–292 (1998).
60. Cornet, S., Nicot, A., Rivero, A. & Gandon, S. Evolution of plastic transmission strategies in avian malaria. *PLoS Pathog.* **10**, e1004308 (2014).

Publisher's note Springer Nature remains neutral with regard to jurisdictional claims in published maps and institutional affiliations.

© The Author(s), under exclusive licence to Springer Nature America, Inc. 2020

Methods

Study individuals and ethical approval. This study, registered at ClinicalTrials.gov (identifier NCT01322581), was approved by the Ethics Committee of Heidelberg University Hospital; the Faculty of Medicine, Pharmacy and Odontostomatology at the University of Bamako; and the National Institute of Allergy and Infectious Diseases of the National Institutes of Health Institutional Review Board. Samples and clinical data were obtained between 2011 and 2019 in a cohort study previously described¹³ and conducted in Kalifabougou, Mali, where malaria transmission occurs from June through December. Access to antimalarial drugs was provided by a single clinic and pharmacy. A random sample of the village population was drawn in an age-stratified manner to enroll the study, including individuals aged 3 months to 45 years. Written informed consent was obtained from all participants and the parents/guardians of included children. Exclusion criteria at enrollment included hemoglobin <7 g dL⁻¹, axillary temperature ≥37.5°C, acute systemic illness or use of antimalarial or immunosuppressive medications in the 30 d preceding enrollment. Clinical malaria cases were determined prospectively by passive surveillance and defined by axillary temperature ≥37.5°C, ≥2,500 asexual parasites per μl of blood and no other apparent cause of fever. Malaria episodes were treated according to Malian national guidelines with a 3-d standard course of artemether and lumefantrine. Cross-sectional clinical visits and blood draws were performed at the beginning (January), mid (March) and end (May) of each dry season.

Sample collection. Dried blood spots on filter paper (Protein Saver 903, Whatman), thick blood smear and venous blood (4 or 8 ml depending on whether donor age was below or above 4 years) were collected on dry season cross-sectional visits and at their first malaria episode of the transmission season. Blood samples drawn by venipuncture were collected in sodium citrate-containing cell preparation tubes (Vacutainer CPT Tubes, BD) and transported to the laboratory where PBMCs, plasma and RBC pellets were separated by centrifugation and used freshly or stored at -80°C within 3 h. An additional 2 ml of venous blood from RDT⁺ individuals who tested at the end of the dry season (May 2012) cross-sectional¹³, and from individuals at their first malaria episode of the ensuing transmission season, was collected into EDTA tubes (Vacutainer K3EDTA Tubes, BD) and processed directly at the field site. Plasma (used for metabolomic analysis) was separated by centrifugation and immediately frozen in liquid N₂. The buffy coat was discarded, and leucocytes were removed from the RBC pellet in a two-step procedure: first by density gradient on Lymphoprep solution (Fresenius Kabi), followed by Plasmodipur (EuroProxima) filtration, all according to the manufacturer instructions and as previously described⁶¹. RBC pellets were then frozen in liquid N₂ and were later used for the RNA-seq and RT-qPCR validation.

Detection of clinical malaria and subclinical *P. falciparum* infection.

Plasmodium parasites per microliter of whole blood were counted in Giemsa-stained thick blood smears against 300 leukocytes of all symptomatic participants presenting to the study clinic, based on a mean leukocyte count of 7,500 cells per μl. Each smear was evaluated separately by two expert microscopists, and a third resolved discrepancies. Subclinical infections during the dry season were detected at cross-sectional time points by RDT (SD BIOLINE Malaria Ag Pf test of histidine-rich protein II) with a sensitivity of ~100 parasites per μl⁶² once the blood was in the laboratory and by Giemsa-stained smear and nested PCR amplification of *P. falciparum* DNA retrospectively as previously described¹³ from filter papers (2017) and frozen RBC pellets (2018). The sensitivity of the nested PCR is ~0.5–1 parasites per μl⁴³.

***P. falciparum* quantification.** By flow cytometry, RBC pellets removed from CPT tubes after leucocyte isolation were washed and stained with 5× SYBR Green I (Invitrogen) and 7.5 μM MitoTracker (Applied Biosystems) for 30 min at 37°C. Cells were acquired using an LSR II and analyzed using FlowJo software 10.2 or higher versions. By RT-qPCR, RNA was extracted immediately after thawing RBC pellets using TRIzol LS (Ambion) according to manufacturer instructions, and complementary DNA (cDNA) was synthesized using SuperScript IV VILO Master Mix with eZDnase (Invitrogen). RT-qPCR was run on a qTower (Analytik Jena) using Power SYBR Green PCR Master Mix (Applied Biosystems) with primers for the *P. falciparum* reference gene glycine-tRNA ligase (PF14_0198) (forward, 5'-TGAGTGATATGGATAATA TAAAGGAACAAA-3'; reverse, 5'-GGATGATATTCAAA ACGTATCTTCT-3') and for human GAPDH (forward, 5'-ACAACTTGGTATCGTGGAAAGG-3'; reverse, 5'-GCCATCACGCCA CAGTTTC-3').

Serologic analyses. CRP, vWF and hepcidin in human plasmas were detected through the CRP Human ELISA Kit (Invitrogen), Human vWF A2 Domain Sandwich ELISA (R&D Systems) and Hepcidin 25 ELISA Kit (DRG Diagnostics), respectively, all according to manufacturer instructions. Results were measured using the Cytaion3 plate reader (BioTek). Milliplex Human Cytokine/Chemokine Magnetic Bead Panel 41-Plex Kit (Merck) was used to measure circulating analytes in human plasma according to manufacturer instructions and read on a Bio-Plex 200 System (Bio-Rad). PfEMP1 domain antibody reactivity was measured using PfEMP1 domains covalently coupled beads following the method described by

Cham et al.⁴⁵. PfEMP1 coupled beads were incubated with diluted plasma samples for 30 min, followed by incubation with 1:3,000 human secondary F(ab')² Goat Anti-Human IgG (Jackson ImmunoResearch) detection antibody for 30 min. The results were read on a Bio-Plex 200 System. The threshold for reactivity of each PfEMP1 domain was calculated with the average value of 21 German controls plus three standard deviations. Reactivity to PfEMP1 A, B and B/A subtypes was determined by the fluorescence intensity of reactive individuals in the beginning (January) and end (May) of the dry season of subclinical carriers and non-infected individuals. Slopes of subclinical carriers and non-infected individuals were compared using a linear non-interaction model.

Processing of PBMCs. PBMCs were isolated from the Vacutainer CPT Tubes according to manufacturer instructions and were either stained and analyzed immediately or frozen within 3 h of the blood draw in FBS containing 7.5% DMSO (FBS: Gibco; DMSO: Sigma-Aldrich). The cells were first frozen at -80°C for 24 h and then subsequently transferred to liquid N₂ for long-term storage. For experiments where PBMCs were used from frozen vials, PBMCs were rapidly thawed in a 37°C water bath, washed with 10% heat-inactivated FBS in PBS, followed by complete RPMI (RPMI 1640 supplemented with 10% heat-inactivated FBS, 1% penicillin-streptomycin and 0.5% β-mercaptoethanol). For each experiment, PBMCs from all individuals were thawed and assayed at the same time. The trypan blue dye exclusion assay consistently demonstrated greater than 80% viability of PBMCs after thawing. Immediately after thawing or after washing if used fresh, 1–2 × 10⁶ PBMCs were incubated for 30 min at 4°C with different combinations of the following fluorescently labeled surface antibodies diluted 1:25 and stained in 50 μl of 4% FBS in PBS: CD14-PE/BV71, CD16-BV421/BV605/BV711, CD19-PETexasRed/ BV421/PerCPcy5.5, CD21-FITC/PE Texas Red/BV421/APC, CD27- FITC/PEcy7/AlexaFluor 700/BV421/BV650/APCcy7, CD3-BV510/BV711/PerCPcy5.5, CD4-FITC/PEcy5/APC, CD8-PEcy7/APCcy7, TCRγδ-PE and CD56-BV510/BV605. After fixing and permeabilizing the cells with FoxP3 Staining Buffer Set (eBioscience) according to manufacturer instructions, PBMCs were stained for 30 min with 1:25 diluted fluorescently labeled intracellular antibodies: CD25-PEcy7, T-bet-PE Texas Red, IL-2-FITC, Granzyme B-PE Texas Red, FCRL5-PE and Granzyme A-AF647. Cells were acquired using BD LSR II or LSR Fortessa flow cytometers (BD) and analyzed using FlowJo 10.2 or higher versions.

Flow cytometry with *P. falciparum*-specific B cell probes. Recently thawed PBMCs were stained with biotinylated recombinant *PfMSP1* and *PfAMA1* and then coupled to fluorescently labeled streptavidin²¹, together with the following labeled monoclonal antibodies: CD3-BV510 (clone UCHT1), CD4-BV510 (clone SK3), CD8-BV510 (RPA-T8), CD14-BV510 (clone M5E2), CD16-BV510 (clone 3G8), CD56-BV510 (clone HCD56), CD10-BUV737 (clone Hi10a), IgD-BUV737 (clone IA-2), CD19-ECD (clone J3-119), CD21-PE-Cy7 (clone B-ly4), CD27-BV605 (clone M-T271), IgM-PerCP-Cy5.5 (clone G20-127) and IgG-AlexaFluor700 (clone G18-145). Aqua Dead Cell Stain was added for live/dead discrimination (Thermo Fisher Scientific). Stained samples were run on a LSR Fortessa X20 (BD), and data were analyzed using FlowJo 10.2 or higher versions. *PfMSP1*- or *PfAMA1*-specific MBCs were identified after exclusion of CD3⁺CD4⁺CD8⁺CD14⁺CD16⁺CD56⁺ non-B cells and CD10⁺ immature and IgD⁻ B cells. To increase the frequency of specific B cells detected in any given sample, PBMCs were stained simultaneously with *PfAMA1* and *PfMSP1* probes. Therefore, *PfAMA1* and *PfMSP1* probe-binding cells are indistinguishable by flow cytometry analysis and are referred to together as 'Pf-specific' cells. Influenza hemagglutinin (HA) antigen was used as a non-Pf-specific cells control.

***P. falciparum* culture.** 3D7 *P. falciparum* parasites were maintained in fresh human O^{Rh+} erythrocytes at 5% hematocrit in RPMI 1640 complete medium (with L-glutamine and HEPES 7.4% sodium bicarbonate, 100 μM hypoxanthine (C.C.Pro) and 25 mg ml⁻¹ gentamycin (all Gibco)) added with 0.25% Albumax II (Gibco), at 37°C either in the presence of a gas mixture containing 5% O₂, 5% CO₂ and 90% N₂ or using the candle jar system method described by Trager and Jensen⁶³.

***P. falciparum* invasion assay.** 3D7 *P. falciparum* parasites were cultured and regularly synchronized by the use of 5% sorbitol⁴⁴ and heparin to prevent re-invasion. At the early schizont stage, E64 compound (Sigma-Aldrich) was used to prevent merozoite egress, and, later, merozoites were purified through filtration as previously described⁴⁶. Merozoites were cultured with non-infected RBCs and RPMI medium supplemented with 25% human plasma from different donors for 30 min to allow invasion, and then RPMI medium supplemented with Albumax II was provided to all parasites for 30 h. iRBCs were fixed as previously described⁶⁶ and stained with 5% SYBR Green, and successful invasion by merozoites was measured 30 h after invasion using FACS Canto II (BD) and analyzed using FlowJo software 10.2 or higher versions. Antibody depletion from human plasma was achieved using Protein G and Protein L Plus Agarose beads (Pierce, Thermo Fisher Scientific). Successful depletion was obtained after three incubations of plasma with the beads and was verified with a Ready-SET-Go! ELISA Kit (eBioscience) measuring total IgG and IgM quantities in the plasma before and after depletion read. Results were read on a Cytaion3 plate reader.

Msp2 fragment analysis by capillary electrophoresis. DNA was extracted from two 3-mm circular punches of blood spots on filter papers (Whatman 3MM), using the DNeasy Blood & Tissue Kit (Qiagen). Genotyping of *msp2* was performed using a previously described nested PCR reaction²⁵. The first PCR amplified the outer *msp2* domain (forward, 5'-ATGAAGGTAAATTAAACATTGTCTTATA-3'; reverse, 5'-CTTGTACACGGTACATTCTT-3'), and the second PCR used fluorescently labeled primers to identify two *msp2* allelic families: IC/3D7 (forward, 5'-AGAAGATGCAGAAAAGAACKCTCYCTACT-3' and reverse, 5'-GATGTAATCGGGGATCAGTTGTC G-3' VIC) and FC27 (FC27 forward, 5'-AATACAAGAGGGCRATGCTCCA-3'; reverse, 5'-TTTATTGGTGCATTGCCAGAACCTGAAC-3' 6-FAM). Fragment analysis was performed by capillary electrophoresis using a DNA sequencer (3730, Applied Biosystems) and analyzed using GeneMapper 5 software (Thermo Fisher Scientific), where a cutoff of 300 relative fluorescent units was set. Fragments were considered to be the same allele within each allelic type if the size difference between them was less than 3 base pairs.

Transcriptome analysis. RNA was extracted from frozen RBC pellets using TRIzol as previously described¹ and was performed from RBC pellets that were frozen in liquid N₂ immediately after blood draw. RNA quality was tested using a Bioanalyzer (Agilent). The average RNA integrity number value was 5.4 for the dry season samples and 5.3 for the clinical malaria cases. The average Bioanalyzer yield was 27.4 ng on the dry season samples, whereas the average Bioanalyzer yield on the clinical malaria cases was 25.0 ng. Twenty-four samples were selected based on parasitemia, the highest 12 titers for the wet and dry seasons. The RNA input going into next-generation sequencing (NGS) sample preparation ranged from 100 pg up to 100 ng. The samples were prepared for transcriptome analysis following a previously described protocol²⁷ with minor modifications. Initially, samples were treated with TURBO DNase as described. After DNase treatment, Agencourt RNAClean SPRI beads (Beckman Coulter) were resuspended in 19 µl to modify the protocol for a low-input ribosomal RNA depletion step. Ribosomal RNA was depleted following the Clontech Modified Protocol for Removal of rRNA from Small Amounts of Total RNA (100 ng) using Human/Mouse/Rat Ribo-Zero Magnetic Kit (Epicentre). The purification beads were resuspended in 21 µl to proceed with the fragmentation step as described²⁷. The first- and second-strand cDNA synthesis steps were followed without modification, except that the final bead purification was eluted in 55 µl. Aliquots from the DNase, Ribo-Zero treatment and fragmentation were analyzed on Agilent Bioanalyzer Pico RNA chips, along with the final cDNA constructs. The purified cDNA was below detectable levels of the Bioanalyzer Pico chips. Next, 50 µl of purified cDNA was prepared for NGS using the KAPA Hyper Prep Kit (KAPA Biosystems). The adaptor stock concentration was 300 nM for the ligation with 4-h incubation at 20°C. The USER digestion step was omitted as the Hi-Fi polymerase does not amplify uracil-containing products. The number of amplification cycles for PCR was determined to be 14 based on quantification of the amount of post-ligation product with a KAPA Quant Kit for Illumina Sequencing (KAPA Biosystems). The purified amplified libraries were visualized on Agilent DNA 1000 chips. Libraries were quantified using the KAPA Quant Kit for Illumina Sequencing and normalized to 2 nM. The samples were pooled based on parasitemias, denatured and diluted to 11 pM for cluster generation and paired-end 100-cycle sequencing on a HiSeq 2500 Rapid flow cell (Illumina) producing ~13 million reads per sample. Raw reads were trimmed of adapter sequence and low-quality bases and filtered for low-quality reads using the FASTX-Toolkit v0.0.14. Remaining reads were mapped to the *P. falciparum* genome, build ASM276v1, using HISAT2 v2.0.4 (ref. ²⁸). Reads mapping to genes were counted using htseq-count: v0.6.1 (ref. ²⁹). For each sample, parasite age (hpi) was estimated based on gene expression using a previously described maximum likelihood method³⁰, applying a script that was kindly provided by Chris Newbold (lemieux_et_al_pipeline_functions.r and lemieux_et_al_pipeline.r). Differential expression analysis was performed using the Bioconductor package DESeq2 v1.26.0 (ref. ²⁰), with adjusted *P* values (*P*_{adj}) < 0.05 considered significant. DEGs were analyzed for enrichment in Gene Ontology categories using DAVID³¹. RNA-seq data (normalized counts data and raw sequencing reads) are available at the National Center for Biotechnology Information's Gene Expression Omnibus (project ID no. GSE148125). Validating RT-qPCR was performed on the 24 above-mentioned samples and on an extra set of 18 samples: six dry season and 12 clinical cases during the wet season. Vilo cDNAs were synthesized using the SuperScript Vilo cDNA Synthesis Kit (Invitrogen) and purified according to QIAquick 96-well protocol (Qiagen) with a modified centrifugation protocol²⁷. Expression levels of eight transcripts (sir2, rex3, Pfsec23, PFB0100c/KARHP, PF07_0006/STARP antigen, PFB0900c/PF1STC GEX20, PF08_0020/UBE4B and MIF) were determined by RT-qPCR using Invitrogen Express qPCR SuperMix with premixed ROX reference dye (Invitrogen) in 20-µl reactions. All gene-specific oligo sequences were designed using Beacon Designer software (Premier Biosoft) and purchased from LGC, Biosearch Technologies, with double quencher BHQnova fluorescent probes owing to AT-rich *P. falciparum* sequences (Supplementary Table 7). In a multiplex format, we used reference gene glycine-tRNA ligase%2C putative (PF14_0198) and a standard made from pooled SPIA cDNA. RT-qPCR reactions were carried out at 95°C for 2 min, 55 cycles of 95°C for 15 s and 60°C for 1 min. Data were

analyzed using the 7900HT version 2.4 sequence detection system software per the manufacturer's recommendations.

Metabolite profiling. Plasma metabolomics was performed using both targeted and untargeted approaches, across several LC-MS platforms, for small molecules and lipids, to obtain full metabolite coverage. Each plasma sample was split into two independent samples for metabolite extraction. For hydrophilic metabolites, 50 µl of plasma was extracted by the addition of 9× volumes of ice-cold methanol. Samples were briefly vortexed before centrifuging for 10 min to remove precipitated protein. The clarified supernatants were dried under N₂ gas and resuspended in 100 µl (1:2 dilution). Sample groups were pooled to create a group quality assurance (QA), and all samples were pooled to create a batch quality control (QC), which were injected periodically throughout each run. The hydrophilic extracts were randomized and analyzed using reverse-phase high-performance LC-MS by injecting 10 µl onto an AB SCIEX 5600 (QTOF) TripleTOF in positive ESI mode before injection on a Thermo Exactive Plus Orbitrap in negative ESI mode. Samples were separated on the AB SCIEX 5600 by reverse-phase HPLC using a Prominence 20 UFLCXR System (Shimadzu) with a Waters (Milford) BEH C18 column (100 mm × 2.1 mm, 1.7-µm particle size) maintained at 55°C and a 20-min aqueous acetonitrile gradient at a flow rate of 250 µl min⁻¹. Solvent A was HPLC-grade water with 0.1% formic acid; solvent B was HPLC-grade acetonitrile with 0.1% formic acid. The initial conditions were 97% A and 3% B, increasing to 45% B at 10 min and 75% B at 12 min where it was held at 75% B until 17.5 min before returning to the initial conditions. The eluate was delivered into a 5600 TripleTOF using a Duospray ion source (all AB SCIEX). The capillary voltage was set at 4.5 kV in negative ion mode, with a declustering potential of 80 V. The mass spectrometer was operated in information-dependent acquisition mode with a 100-ms survey scan from 100 to 1,200 m/z and up to 20 MS/MS product ion scans (100 ms) per duty cycle using a collision energy of 50 V with a 20-V spread. Metabolite separation was performed on the Thermo Exactive Plus Orbitrap as previously described³ using a Waters XSelect HSS T3 column (2.1 × 100 mm, 2.5 µm). For hydrophobic metabolites, 25 µl of plasma was extracted by the addition of 3× volumes of isopropanol. Samples were briefly vortexed and allowed to sit at room temperature for 10 min. Samples were then placed at -20°C to precipitate overnight. Precipitated samples were centrifuged for 20 min, and the clarified supernatant was diluted to 50% water in a glass LC-MS sample vial (1:6 dilution). Sample groups were pooled to create a group QA, and all samples were pooled to create a batch QC, which were injected periodically throughout each run. The hydrophobic extracts were randomized and analyzed using reverse-phase high-performance LC-MS by injecting 10 µl of sample onto an AB SCIEX 5600 TripleTOF in positive and negative ESI modes. Metabolite separation was performed as previously described⁴ using a Waters Acuity UPLC CSH C18 column (100 × 2.1 mm, 1.7 µm). Ammonium formate and formic acid were added to the positive ESI solvents, and ammonium acetate was used for negative ESI. Targeted analysis of the Orbitrap data was performed as previously described²⁵. Untargeted analysis from the 5600 TripleTOF was performed using the default settings in MS-DIAL²⁶. The built-in databases were used for putative identification of metabolites at the MS/MS level. QA/QC samples were evaluated to minimize systematic and technical issues. All data were normalized to the total ion chromatogram and blank subtracted, to remove background noise, before statistical analysis.

***P. falciparum* field isolates short-term culture.** RBC pellets isolated from CPT tubes of RDT⁺ samples in the dry season and of malaria case samples in the transmission season were cultured in fresh human O^{Rh+} erythrocytes at 7% hematocrit in complete RPMI supplemented with 0.25% Albumax II at 37°C in a candle jar for 36 or 48 h. Malaria case samples were cultured undiluted and diluted 1:10, 1:25 and 1:50 with non-infected blood to assure that initial parasitemia was low (0.5–1%) and that all cultured parasites could grow to their maximum potential. Parasitemia and parasite development were assessed at 0, 16, 24, 30, 36 and 48 h in culture by thin blood smears and flow cytometry. Parasitemia fold change was determined for each sample (ratio of %iRBCs at each time point over its preceding one). The time of highest increase of parasitemia was the time point at which the ratio of %iRBCs at a given time point over its preceding one was the highest for each sample. Progeny number was determined by dividing SYBR Green fluorescence of multi-nucleated schizonts before or at the time of the highest increase in parasitemia in vitro by the fluorescence of the smallest ring stage population that sample presented. Fiji software was used to measure *P. falciparum* area.

Microfiltration of *P. falciparum* iRBCs. RBC pellets isolated from CPT tubes of RDT⁺ samples in the dry season and of malaria cases samples in the transmission season were leucocyte depleted using EasySep CD45 Depletion Kit (STEMCELL Technologies), according to manufacturer instructions. iRBCs were cultured in complete RPMI medium supplemented with Albumax, and microfiltration was performed in triplicates at 0, 6, 18 and 30 h in culture as previously described²⁹. Briefly, calibrated microspheres of 5–15 µm and 15–25 µm in diameter (S96.5% tin, 3% silver, 0.5% copper; Industrie des Poudres Sphériques) were mixed at 4 g each in 12 ml of complete medium. Filter tips (732–0534, VWR) were cut

diagonally on the tip and wet by pushing 200 μl of complete medium through the filter. The bead suspension was vortexed, and 400 μl was loaded onto the filter tips, yielding a 1.5-mm layer of microsphere beads. The tips were then filled up with medium and connected to a three-way stopcock. Microfiltration tips were used within 12 h of preparation. At each time point, 600 μl of the 2% hematocrit culture was loaded onto the microbead layer and perfused with 5 ml of complete medium at 1 ml min⁻¹ using a syringe pump (AL-4000, World Precision Instruments). The upstream and downstream samples were collected at the different time points and stained for *P. falciparum* quantification by flow cytometry. Samples in which parasitemia increased (fold change > 1) between 0 and 30 h (May) or 0 and 48 h (MAL) were included in the analysis.

Simulation of *P. falciparum* cyto-adhesion and splenic clearance. We developed a discrete-time within-host infection model to monitor parasite replication, cyto-adhesion and splenic clearance in the absence of host immune responses. The parasite's 48-h life cycle was divided into eight 6-h time steps, and we assumed that the parasite population was fully synchronized. The dynamics of circulating, B_i , and cyto-adhering, V_i , parasites are described through the following iterative scheme

$$\begin{aligned} B_0^{t+1} &= \gamma(B_0^t + V_8^t) \\ B_1^{t+1} &= (1 - \sigma_1)(1 - \eta_1)B_0^{t+1} \\ V_1^{t+1} &= \eta_1 B_0^{t+1} \\ B_i^{t+1} &= (1 - \sigma_i)(1 - \eta_i)B_{i-1}^{t+1}, \quad \forall i \in [2, 3, \dots, 8] \\ V_i^{t+1} &= \eta_i B_{i-1}^{t+1} + V_{i-1}^{t+1}, \quad \forall i \in [2, 3, \dots, 8] \end{aligned}$$

where B_i^t and V_i^t are the numbers of circulating and cyto-adhering parasites of age i and at time t , respectively. γ is the intrinsic parasite growth rate—that is, the average number of newly infected RBCs arising from a single infected cell. As seen from the above equations, only cyto-adhering and freely circulating iRBCs replicate and contribute to parasite population growth, whereas the spleen is assumed to remove retained parasites. Removal of infected RBCs from circulation by means of cytoadhesion, η_i , and splenic clearance, σ_i , is assumed to be dependent on the age of the parasite, i , where the rate of removal increases as the parasite starts to express cyto-adhering VSAs, PfEMP1, shortly after invasion, and where RBC modification by the parasite gradually increases the cell's rigidity and, hence, splenic retention. Both removal functions are given by the following sigmoidal forms

$$\begin{aligned} \sigma_i &= \sigma(i) = \frac{\sigma_{\max}}{1 + e^{p_{\sigma} \times (T_{\sigma} - i)}} \\ \eta_i &= \eta(i) = \kappa \frac{\eta_{\max}}{1 + e^{p_{\eta} \times (T_{\eta} - i)}} \end{aligned}$$

and are visualized in Extended Data Fig. 7. σ_{\max} and η_{\max} are the maximum removal rates by the spleen and cyto-adhesion, respectively. p_{σ} and T_{σ} are the shape and location parameters of the sigmoidal functions, where T determines the age at which 50% of the parasites are removed. The factor $\kappa \in [0, 1]$ is included to investigate the effect of cyto-adhesion on the within-host growth dynamics. All parameters and values used are listed in Supplementary Table 12.

PfEMP1 genes expression. To exclude human reads, all reads were mapped against the human genome (hg19) using bwa mem⁷ (-k 32). Reads and their pair that did not map the human genome were used further. Reads were correct with quorum⁷⁸, parameter -k 35. Adapters were trimmed with cutadapt⁷⁹, using the TruSeq LT adapter sequences. To assemble the *var* genes, the RNA-seq reads (fastq files) were first assembled with the pipeline recently published in Otto et al.³¹. Owing to the variable coverage of the sequence reads, the results were not satisfactory. Therefore, an older approach was used to assemble all the non-human sequencing reads with velvet⁸⁰, following parameters Kmer 41, exp_cov 99999999, ins_length 420, cov_cutoff 5, ins_length_sd 30 and min_pair_count 5. Different k-mer were tested, and k-mer of 41 returned the best results. The obtained contigs were annotated, and the domains were called as previously described³¹. For each *var* gene, domains and subdomains were annotated as defined by Rask et al. (vardom⁸¹). The expression per *var* gene was calculated with two methods. In both methods, the reads back with bwa mem were mapped against the assemblies. In the first method, the number of mapped reads was counted on *var* genes larger than 3,500 and normalized by the length of the *var* genes and the number of reads mapped against all contigs, similar to RPKM. In the second method, the coverage over the middle of the LARSFADIG motifs (samtools depth) was addressed. These values were divided by the number of reads mapped on each assembly and multiplied by 10 million. As a complementary validation, a mapping approach was used: the sequencing reads were mapped using bwa mem, parameter -k 31 -a (to allow multiple hits), against a combined database of *var* genes from Otto et al.³¹ (varDB, fulldataset.1kb.nt.fasta.gz) and the *var* genes from Otto et al.⁸², limited to *var* genes of the length of at least 3 kb. Next, the number of reads mapped with an AS score of at least 95 against the *var* genes from this combined database were counted.

Statistical analysis. Mann–Whitney or Kruskal–Wallis was used to test for differences between two or more groups, respectively. Differences between the number of clones and clone sizes were tested by Mood's median test. PfEMP1 slopes between the beginning and the end of the dry season of subclinical carriers

and non-infected individuals were compared using a linear non-interaction model. Spearman's rank correlation between linear RT-qPCR normalized data and linear RNA-seq normalized data of each gene was obtained along with P values using GraphPad Prism 8.0 software. Metabolite significant differences were determined by a two-way analysis of variance (ANOVA) corrected for multiple comparisons controlling for a false discovery rate of 0.05%. Statistical significance was defined as a two-tailed P value of ≤ 0.05 . All analyses were performed with GraphPad Prism versions 6.0 or 8.0, JMP 14.0.1 or R.

Reporting Summary. Further information on research design is available in the Nature Research Reporting Summary linked to this article.

Data availability

RNA-seq data (normalized counts data and raw sequencing reads) have been deposited in the National Center of Biotechnology Information's Gene Expression Omnibus (GEO) and are accessible through GEO Series accession number GSE148125.

Metabolomics data are available at the National Institutes of Health (NIH) Common Fund's National Metabolomics Data Repository website, the Metabolomics Workbench, <https://www.metabolomicsworkbench.org>, where it has been assigned project ID PR000948. The data can be accessed directly via <https://doi.org/10.21228/M8540T>. This work is supported by NIH grant U2C-DK119886. The data file of assembled *var* gene fragments of all isolates is available at https://github.com/ThomasDOtto/varDB/tree/master/Otherdatasets/Andrade_DryWet2020

References

61. Auburn, S. et al. An effective method to purify *Plasmodium falciparum* DNA directly from clinical blood samples for whole genome high-throughput sequencing. *PLoS ONE* **6**, e22213 (2011).
62. Ratsimbason, A. et al. Evaluation of two new immunochromatographic assays for diagnosis of malaria. *Am. J. Trop. Med. Hyg.* **79**, 670–672 (2008).
63. Trager, W. & Jensen, J. B. Human malaria parasites in continuous culture. *Science* **193**, 673–675 (1976).
64. Radfar, A. et al. Synchronous culture of *Plasmodium falciparum* at high parasitemia levels. *Nat. Protoc.* **4**, 1899–1915 (2009).
65. Boyle, M. J. et al. Isolation of viable *Plasmodium falciparum* merozoites to define erythrocyte invasion events and advance vaccine and drug development. *Proc. Natl Acad. Sci. USA* **107**, 14378–14383 (2010).
66. Tonkin, C. J. et al. Localization of organellar proteins in *Plasmodium falciparum* using a novel set of transfection vectors and a new immunofluorescence fixation method. *Mol. Biochem. Parasitol.* **137**, 13–21 (2004).
67. Broadbent, K. M. et al. Strand-specific RNA sequencing in *Plasmodium falciparum* malaria identifies developmentally regulated long non-coding RNA and circular RNA. *BMC Genomics* **16**, 454 (2015).
68. Kim, D., Langmead, B. & Salzberg, S. L. HISAT: a fast spliced aligner with low memory requirements. *Nat. Methods* **12**, 357–360 (2015).
69. Anders, S., Pyl, P. T. & Huber, W. HTSeq—a Python framework to work with high-throughput sequencing data. *Bioinformatics* **31**, 166–169 (2015).
70. Love, M. I., Huber, W. & Anders, S. Moderated estimation of fold change and dispersion for RNA-seq data with DESeq2. *Genome Biol.* **15**, 550 (2014).
71. Huang da, W., Sherman, B. T. & Lempicki, R. A. Systematic and integrative analysis of large gene lists using DAVID bioinformatics resources. *Nat. Protoc.* **4**, 44–57 (2009).
72. Virtaneva, K. et al. Longitudinal analysis of the group A *Streptococcus* transcriptome in experimental pharyngitis in cynomolgus macaques. *Proc. Natl Acad. Sci. USA* **102**, 9014–9019 (2005).
73. Schalkwijk, J. et al. Antimalarial pantothenamide metabolites target acetyl-coenzyme A biosynthesis in *Plasmodium falciparum*. *Sci. Transl. Med.* **11**, eaas9917 (2019).
74. Cajka, T. & Fiehn, O. Increasing lipidomic coverage by selecting optimal mobile-phase modifiers in LC–MS of blood plasma. *Metabolomics* **12**, 34 (2016).
75. Allman, E. L., Painter, H. J., Samra, J., Carrasquilla, M. & Llinás, M. Metabolomic profiling of the malaria box reveals antimalarial target pathways. *Antimicrob. Agents Chemother.* **60**, 6635–6649 (2016).
76. Tsugawa, H. et al. MS-DIAL: data-independent MS/MS deconvolution for comprehensive metabolome analysis. *Nat. Methods* **12**, 523–526 (2015).
77. Li, H. Aligning sequence reads, clone sequences and assembly contigs with BWA-MEM. Preprint at <https://arxiv.org/abs/1303.3997> (2013).
78. Marcais, G., Yorke, J. A. & Zimin, A. QuorUM: an error corrector for Illumina reads. *PLoS ONE* **10**, e0130821 (2015).
79. Martin, M. Cutadapt removes adapter sequences from high-throughput sequencing reads. *EMBNet J.* **17**, 10–12 (2011).

80. Zerbino, D. R. in *Current Protocols in Bioinformatics* (ed Baxevanis, A. D.) (John Wiley and Sons, 2010).
81. Rask, T. S., Hansen, D. A., Theander, T. G., Gorm Pedersen, A. & Lavstsen, T. *Plasmodium falciparum* erythrocyte membrane protein 1 diversity in seven genomes—divide and conquer. *PLoS Comput. Biol.* **6**, e1000933 (2010).
82. Otto, T. D. et al. Long read assemblies of geographically dispersed *Plasmodium falciparum* isolates reveal highly structured subtelomeres. *Wellcome Open Res.* **3**, 52 (2018).

Acknowledgements

We thank the residents of Kalifabougou, Mali, for participating in this study. We acknowledge the support of the Flow Cytometry Core Facility of DKFZ in Heidelberg, Germany, and the Immunology Core Lab of the UCRC in Bamako, Mali. We thank the Metabolomics Core Facility at Penn State University and A. Patterson and P. Smith from the Penn State Metabolomics Core. We thank Z. Bozdech and the lab at Nanyang Technological University, Singapore, for help and expertise with RNA extraction. This work was supported by the German Center for Infection Research (DZIF), the European Research Council under the European Union's Horizon 2020 Research and Innovation Programme (grant agreement 759534), the Deutsche Forschungsgemeinschaft (DFG, German Research Foundation) projektnummer 240245660 SFB 1129 of the German Research Foundation and the Division of Intramural Research, National Institute of Allergy and Infectious Diseases, of the National Institutes of Health. R.T.L. was funded by the European Union's Horizon 2020 Research and Innovation Programme under Marie Skłodowska-Curie grant agreement DLV-839998.

Author contributions

C.M.A., H.F., R.T.-L., N.F.L., C.A., J.H., C.S.H., S.L., M.N., H.C., D.S., C.M., S.R., K.V., M.V.H., E.L.A. and S.P. performed experiments and analyzed data. S.D., D.D., K.K., A.O., B.T. and P.D.C. designed, conducted and supervised field work generating the clinical data and samples. J.M., N.O.S. and T.D.O. performed bioinformatic analysis. M.-E.N., C.L., T.L., M.A., A.F. and M.L. provided technical expertise, and T.L. and L.T. provided essential reagents. M.R. performed mathematical models. T.M.T., J.S. and V.W. provided statistics expertise. C.M.A. prepared figures, and C.M.A., H.F., R.T.-L., T.M.T., N.S.O. and T.D.O. helped prepare the manuscript. T.M.T., A.F., M.L., T.L., T.D.O., M.R. and P.D.C. provided insightful comments to the manuscript. P.D.C. discussed initial field and study designs. S.P. designed the study and wrote the manuscript. All authors read and approved the final manuscript.

Competing interests

The authors declare no competing interests.

Additional information

Extended data is available for this paper at <https://doi.org/10.1038/s41591-020-1084-0>.

Supplementary information is available for this paper at <https://doi.org/10.1038/s41591-020-1084-0>.

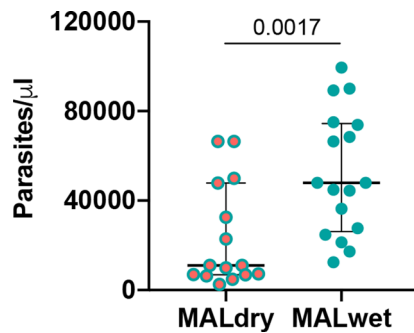
Correspondence and requests for materials should be addressed to S.P.

Peer review information Alison Farrell is the primary editor on this article and managed its editorial process and peer review in collaboration with the rest of the editorial team.

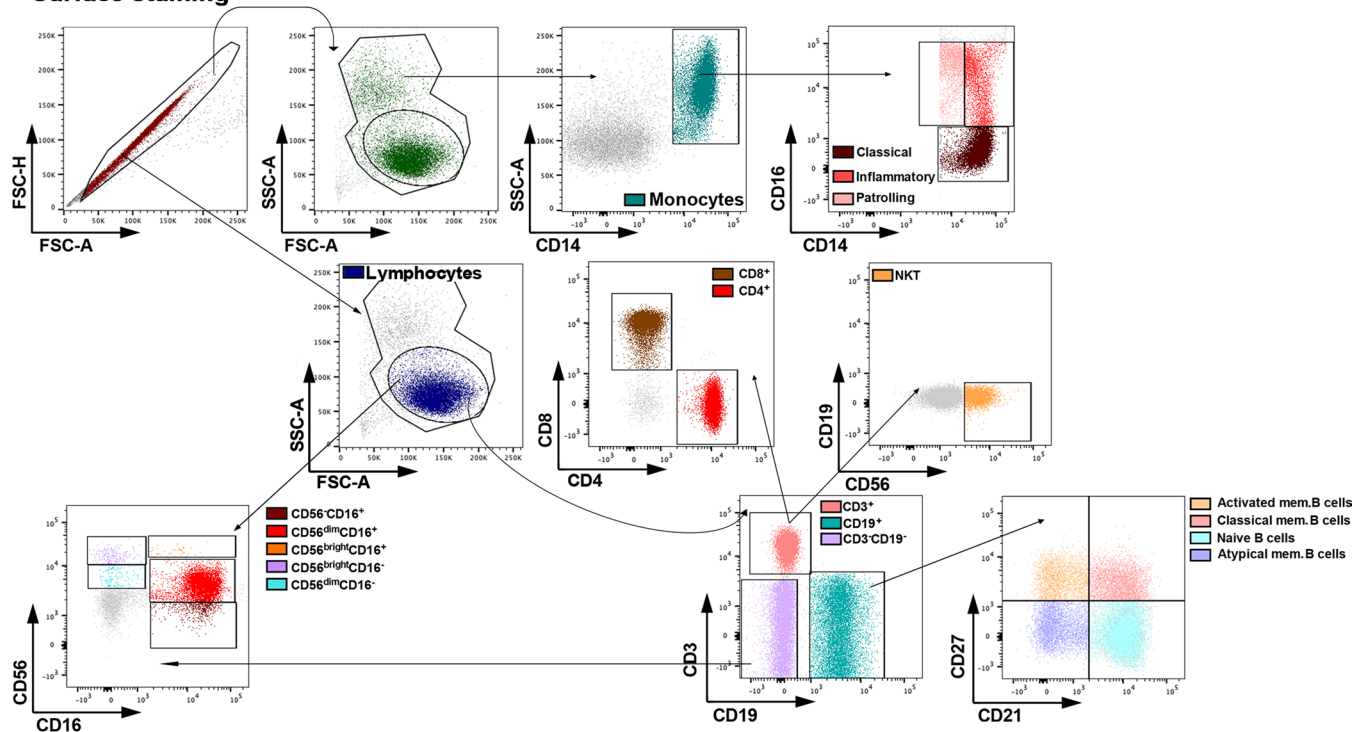
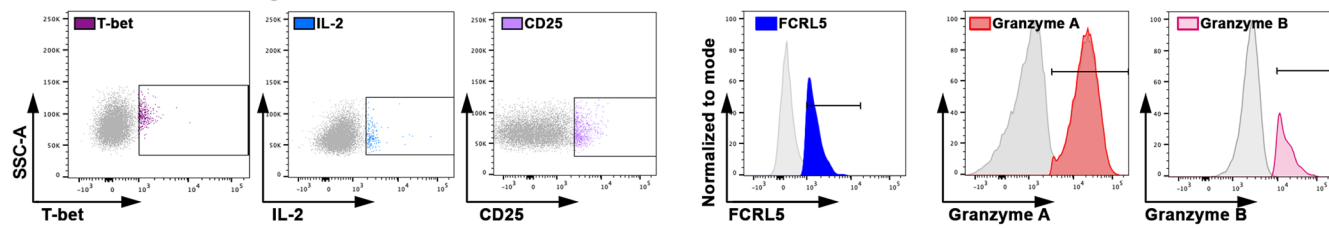
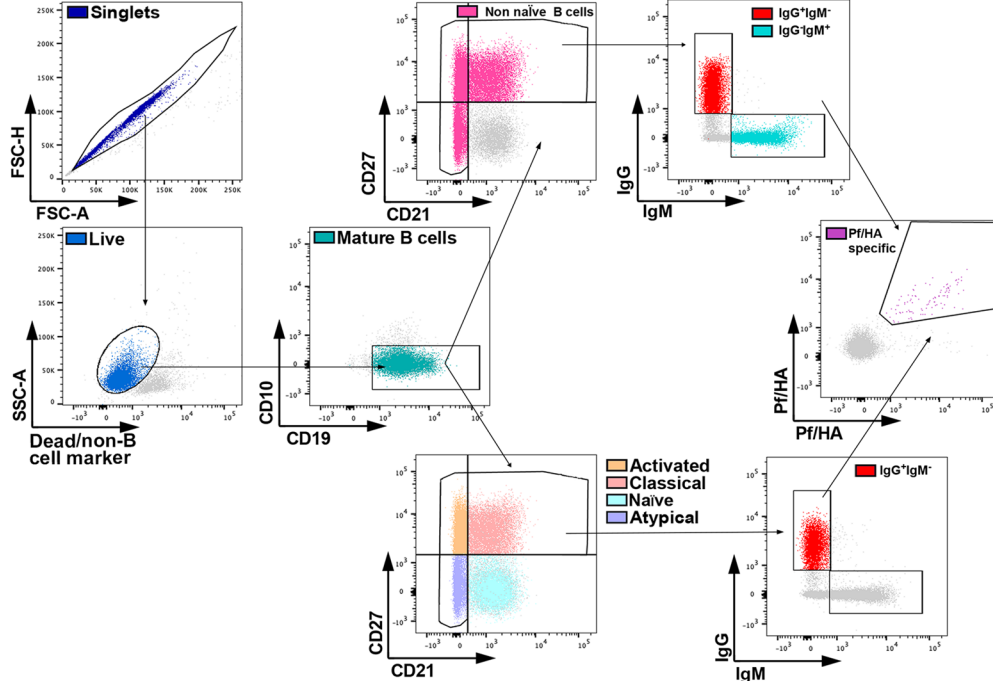
Reprints and permissions information is available at www.nature.com/reprints.

all			MAL		May	
n	female %	Age, y, mean (95% CI)	Malaria cases n	Age malaria case (y, 95% CI)	% Pf+ in May n	Age %Pf+ in May (y, 95% CI)
2017	604	46,7	11.2 (10.5 - 11.8)	398	9.4 (8.8 - 10.1)	13,4
2018	603	46,3	10.8 (10.1 - 11.5)	352	9.2 (8.5 - 10.0)	10,9

Extended Data Fig. 1 | Characteristics of study participants stratified by year.

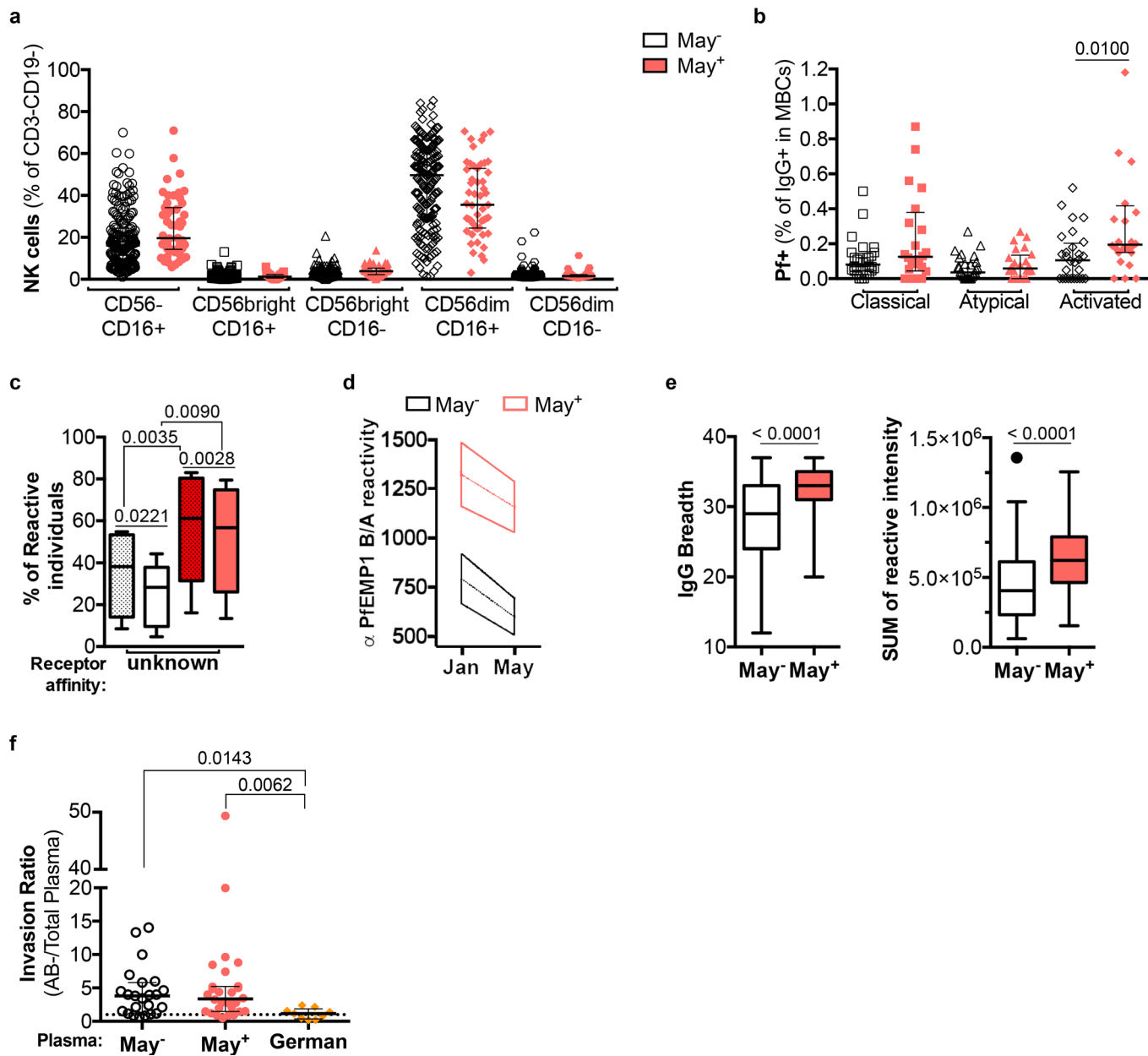


Extended Data Fig. 2 | Parasite density of malaria cases during dry and transmission seasons. Parasite density detected by microscopy on thick blood smear of 17 individuals that presented malaria cases both in the dry season (January to May, MALdry) and in the ensuing wet season (June to December, MALwet) in the years on 2017 and 2018. Parasitaemia data shows median \pm IQR, two-tailed Mann-Whitney test.

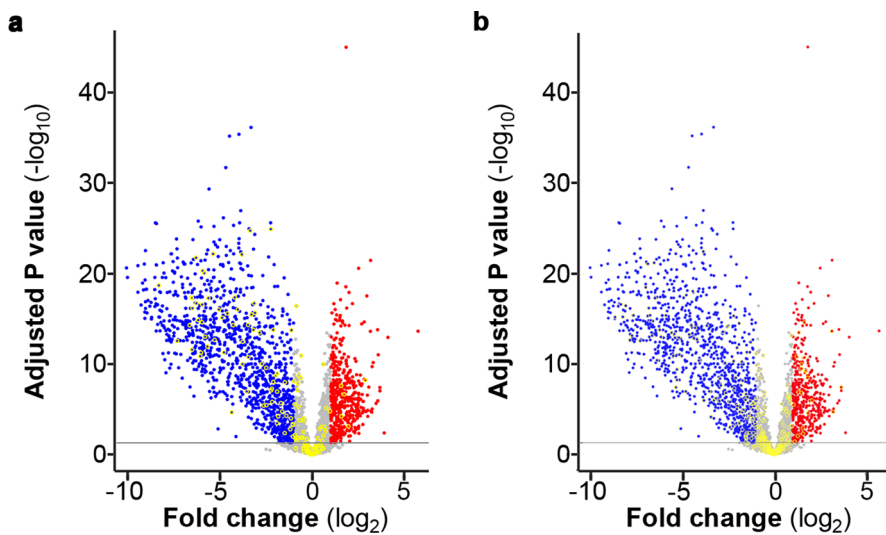
a Surface staining**Intracellular staining****b**

Extended Data Fig. 3 | See next page for caption.

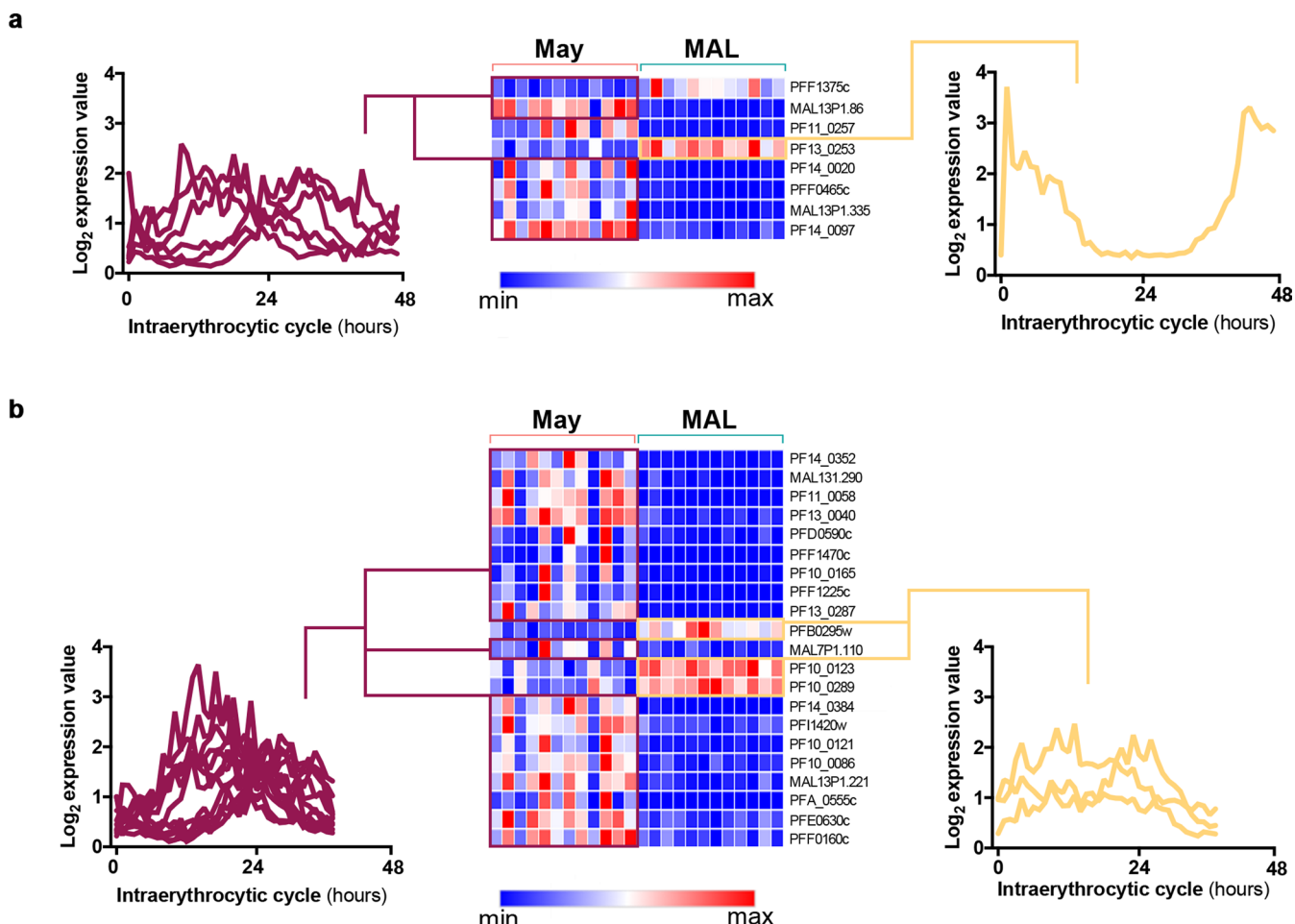
Extended Data Fig. 3 | Flow cytometry gating strategies. **a**, Major leucocyte populations from frozen and fresh PBMCs (Surface staining) and fresh PBMCs intracellular content (Intracellular staining). **b**, *P. falciparum*-specific memory B cells in frozen PBMCs at the end of the dry season of children with or without subclinical *P. falciparum* infection.



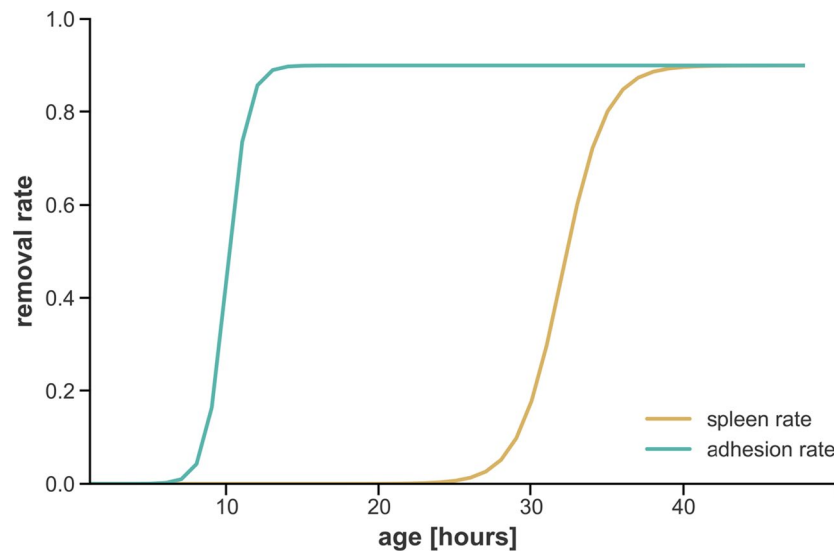
Extended Data Fig. 4 | Immune responses to *P. falciparum* during the dry season. **a**, Proportions of NK subpopulations defined by CD56 and CD16 in children carrying (May⁺) or not (May⁻) *P. falciparum* at the end of the dry season. Median \pm IQR; One sided Dunn's Kruskal-Wallis Multiple Comparisons test. **b**, Proportion of *P. falciparum*-specific IgG⁺ MBCs in classical, activated or atypical MBCs of *P. falciparum* carriers (May⁺) or uninfected individuals (May⁻) at the end of the dry season. Median \pm IQR; One sided Dunn's Kruskal-Wallis Multiple Comparisons test. **c**, Proportion of children with antibodies specific to PfEMP1 domains binding to unknown receptors at the beginning (Jan) and end (May) of the dry season (n=106 Jan and May⁻, 112 Jan and May⁺). Boxplots indicate median \pm IQR. Values >1.5 times the IQR are plotted as individual points (Tukey method), RM one-way ANOVA (with Greenhouse-Geisser correction). **d**, Magnitude of IgG antibodies against PfEMP1 domains of B/A subtype between the beginning and end of the dry season in children carrying (May⁺) or not (May⁻) subclinical *P. falciparum* infection at the end of the dry season (n=106 Jan and May⁻, 112 Jan and May⁺). **e**, Breadth (left) and magnitude (right) of IgG reactivity to invasion-related antigens (Supplementary Table 11) at the end of the dry season in non-infected and subclinical children carrying *P. falciparum* (n=143 May⁻, 139 May⁺). Individual antigen reactivity (detailed in Portugal et al.¹³) of invasion-related antigens based on Cowman et al.²³. Breadth is the number of antigens to which the level of IgG reactivity exceeds 2 SDs above the no DNA control. Magnitude is the sum of log2 -IgG intensity values for all antigens per sample. Boxplots indicate median \pm IQR, Tukey method, two-tailed Mann-Whitney test. **f**, *P. falciparum* invasion ratio between merozoite invasion in antibody depleted plasma and merozoite invasion in paired complete plasma from subclinical carriers and non-infected children (n=28 May⁺, 23 May⁻), and malaria-naïve control (German adults' plasma, n=9). One sided Dunn's Kruskal-Wallis Multiple Comparisons test.



Extended Data Fig. 5 | Volcano plots comparing the DEGs found in this study with the DEGs reported in two other studies^{26,27}. **a**, 141 DEGs previously reported in the comparison of transcriptomes of severe vs moderate malaria parasite physiological states were matched to the present study. 69 were not DEG in the dry season, 67 were upregulated and 5 were downregulated. **b**, 306 DEGs previously reported in the comparison of high vs low transmission clinical malaria causing parasites were matched to the present study. 182 were not DEGs in the dry season, 103 were upregulated and 21 were downregulated. DEGs found in this study are highlighted in yellow. Dots in blue represent the transcripts up-regulated (1131) and in red the transcripts down-regulated (476) in the dry season compared to clinical malaria samples.



Extended Data Fig. 6 | Expression patterns in 3D7 parasites along the ~48 h intraerythrocytic developmental cycle (defined by Bozdech et al. PLoS Biology, 2003) of DEGs between *P. falciparum* of asymptomatic carriers at the end of the dry season (May) and at the first clinical malaria case (MAL) in the ensuing transmission season. a, Glycerophospholipid metabolism b, Purine and Pyrimidine metabolism pathways by KEGG enrichment analysis using the DAVID tool.



Extended Data Fig. 7 | Modelled removal of infected RBCs from circulation by means of cytoadhesion and splenic clearance over the 48 h replicative cycle, assuming the rate of removal increases with increasing expression of cytoadhering variant surface antigens, and where RBC modification by the parasite gradually increases the cell's rigidity and hence splenic retention.

SampleID	de novo assembly					Mapped base approach		
	total length in bp	# contigs	#LARSFADIG	Max expression	longest contig in bp	# varDB hits	Id of var gene with highest hit	Domain structure of highest hit
May 9307	18.920	10	1	50	6.763	2.693	PF0159-C.g637	NTS-DBLa-CIDRa-DBLb-DBLg-DBLd-CIDRb-DBLb-DBLg-
May 9308	9.624	5	1	37	5.348	14	PF0145-C.g513	NTS-DBLa-CIDRa-DBLd-CIDRb-
May 9309	1.296	2	0	NA	670	13	PF0084-C.g173	NTS-DBLa-CIDRa-DBLd-CIDRb-
May 9310	18.769	10	3	87	6.227	216	PF0043-C.g402	DBLd-CIDRb-
May 9311	2.292	1	0	NA	2.292	14	PT0294-C.g1327	DBLa-CIDRa-DBLb-DBLg-DBLd-CIDRb-DBLb-DBLg-
May 9312	20.556	18	1	30	3.170	64	PF0051-C.g887	DBLa-CIDRa-DBLd-CIDRb-
May 9313	4.721	8	0	NA	2.292	6	PT0122-C.g1412	NTS-DBLa-CIDRa-DBLb-DBLz-DBLg-
May 9314	39.049	28	2	66	9.011	248	PF0262-C.g611	DBLb-DBLb-DBLd-CIDRg-
May 9315	5.824	3	1	307	4.176	193	PF0062-C.g430	NTS-DBLa-CIDRa-DBLd-CIDRb-
May 9316	9.185	13	0	NA	3.400	121	PA0182-C.g826	NTS-DBLa-CIDRa-
May 9317	19.689	20	2	176	5.234	915	PM0098-C.g1086	NTS-DBLa-CIDRa-DBLd-CIDRg-
May 9318	10.131	10	1	55	6.004	51	PF0417-C.g422	NTS-DBLa-CIDRa-DBLd-CIDRb-
MAL 9319	173.674	133	24	159	10.423	1.299	PA0146-C.g1029	DBLd-CIDRb-
MAL 9320	8.666	20	0	NA	2.208	66	PA0224-C.g312	DBLa-CIDRa-DBLd-CIDRb-
MAL 9321	23.668	12	2	1.263	9.564	1.149	PF0097-C.g294	NTS-DBLa-CIDRa-DBLb-DBLg-DBLd-CIDRb-
MAL 9322	138.491	170	16	104	10.046	846	PA0092-C.g461	DBLd-CIDRg-DBLg-DBLz-
MAL 9323	35.909	43	5	48	3.571	103	PA0253-C.g804	NTS-DBLa-CIDRa-DBLd-CIDRb-
MAL 9324	43.517	56	5	27	4.626	136	PF0189-C.g397	DBLd-CIDRb-
MAL 9325	3.849	1	0	NA	3.849	391	PF0801-C.g1202	DBLg-DBLz-DBLg-DBLb-
MAL 9326	113.437	87	17	71	8.812	785	QG0212-C.g1592	NTS-DBLa-CIDRa-DBLd-CIDRb-
MAL 9327	11.330	14	2	109	4.225	82	PA0237-C.g706	NTS-DBLa-CIDRa-DBLd-CIDRb-
MAL 9328	12.501	16	1	163	2.688	63	PF0228-C.g1045	CIDRa-DBLd-CIDRb-
MAL 9329	122.076	120	17	1.140	9.161	1.288	PA0167-C.g886	NTS-DBLa-CIDRa-DBLd-CIDRg-
MAL 9330	106.347	87	13	85	11.752	420	PT0211-C.g738	NTS-DBLa-CIDRa-DBLb-DBLd-CIDRb-

Extended Data Fig. 8 | LARSFADIG motifs that identify PfEMP1 coding genes of 12 subclinical individuals at the end of the dry season (May) and 12 first clinical malaria episodes in the ensuing wet season (MAL).

Reporting Summary

Nature Research wishes to improve the reproducibility of the work that we publish. This form provides structure for consistency and transparency in reporting. For further information on Nature Research policies, see [Authors & Referees](#) and the [Editorial Policy Checklist](#).

Statistics

For all statistical analyses, confirm that the following items are present in the figure legend, table legend, main text, or Methods section.

n/a Confirmed

- The exact sample size (n) for each experimental group/condition, given as a discrete number and unit of measurement
- A statement on whether measurements were taken from distinct samples or whether the same sample was measured repeatedly
- The statistical test(s) used AND whether they are one- or two-sided
Only common tests should be described solely by name; describe more complex techniques in the Methods section.
- A description of all covariates tested
- A description of any assumptions or corrections, such as tests of normality and adjustment for multiple comparisons
- A full description of the statistical parameters including central tendency (e.g. means) or other basic estimates (e.g. regression coefficient) AND variation (e.g. standard deviation) or associated estimates of uncertainty (e.g. confidence intervals)
- For null hypothesis testing, the test statistic (e.g. F , t , r) with confidence intervals, effect sizes, degrees of freedom and P value noted
Give P values as exact values whenever suitable.
- For Bayesian analysis, information on the choice of priors and Markov chain Monte Carlo settings
- For hierarchical and complex designs, identification of the appropriate level for tests and full reporting of outcomes
- Estimates of effect sizes (e.g. Cohen's d , Pearson's r), indicating how they were calculated

Our web collection on [statistics for biologists](#) contains articles on many of the points above.

Software and code

Policy information about [availability of computer code](#)

Data collection

Data included in Fig. 5e was obtained using a likelihood-based statistical method previously described by Lemieux et al., the script (lemieux_et_al_pipeline_functions.r and lemieux_et_al_pipeline.r) was kindly provided by Chris Newbold via Alfred Cortes. All bio-informatics data was obtained using code freely available and we can make all code available too to any interested reader. GeneMapper 4.0 and 5.0 software was used to determine MSP2 sizes in peaks detected by capillary electrophoresis. FACS Diva version 8.0.2 was used to collect flow cytometry data.

Data analysis

Statistical analyses were performed with Graph Pad Prism versions 6.0 or 8.0, JMP 14.0.1, or R3.5.2 as detailed in the methods. FlowJo software 10.2 or higher versions were used for flow cytometry analysis. RNA seq data was analysed using Hisat2 v 2.0.4, Bioconductor package Deseq2 v 1.26.0, Htseq-count v 0.6.1 and FASTX-Toolkit v 0.0.14.

For manuscripts utilizing custom algorithms or software that are central to the research but not yet described in published literature, software must be made available to editors/reviewers. We strongly encourage code deposition in a community repository (e.g. GitHub). See the Nature Research [guidelines for submitting code & software](#) for further information.

Data

Policy information about [availability of data](#)

All manuscripts must include a [data availability statement](#). This statement should provide the following information, where applicable:

- Accession codes, unique identifiers, or web links for publicly available datasets
- A list of figures that have associated raw data
- A description of any restrictions on data availability

Data availability

RNA-Seq data (normalized counts data and raw sequencing reads) have been deposited in NCBI's Gene Expression Omnibus and are accessible through GEO Series accession number GSE148125 (<https://www.ncbi.nlm.nih.gov/geo/query/acc.cgi?acc=GSE148125>)

Metabolomics data is available at the NIH Common Fund's National Metabolomics Data Repository (NMDR) website, the Metabolomics Workbench, <https://www.metabolomicsworkbench.org> where it has been assigned Project ID PR000948. The data can be accessed directly via its Project DOI: doi: 10.21228/M8540T.

This work is supported by NIH grant U2C-DK119886.
 The data file of assembled var gene fragments of all isolates are available at: https://github.com/ThomasDOtto/varDB/tree/master/Otherdatasets/Andrade_DryWet2020
 As detailed in the Data availability section of the manuscript.

Field-specific reporting

Please select the one below that is the best fit for your research. If you are not sure, read the appropriate sections before making your selection.

- Life sciences Behavioural & social sciences Ecological, evolutionary & environmental sciences

For a reference copy of the document with all sections, see nature.com/documents/nr-reporting-summary-flat.pdf

Life sciences study design

All studies must disclose on these points even when the disclosure is negative.

Sample size	No statistical method was used to predetermine sample size. The study included ~600 individuals every year and all clinical data presented in Fig. 1a-c and Supplementary Table 1 include data from all individuals participating in those years with data for each analysis. The decision of size of the study was made based on outcomes of the clinical studies not related with this manuscript. Within the experiments presented in this article no sample size calculations were performed. For data in Fig. 2c-f, Fig 3, and Fig. 5a and c, the number of donor samples used in each experiment was from a minimum of 10 children per group to all the subjects possible to include in each time-point out of the 600 total, during the different cross-sectional time points or during the visit to Bamako in the transmission season, allowing to make the comparisons age- and gender- matched, which was estimated based on our preliminary experiments and previous experience. For all other experiments, a minimum of 10 patient samples were chosen as a sample size to ensure adequate power, unless stated otherwise. Data obtained from each patient sample represents an independent experiment.
Data exclusions	There is no exclusion based on race, ethnicity, or gender. Pre-established exclusion criteria at enrolment in May consisted of haemoglobin concentration <7 g/ dL, axillary temperature >37.5°C, acute systemic illness, or use of antimalarial or immunosuppressive medications in the preceding 30 days. Pregnant women were excluded because of the increased risk of anemia during pregnancy and the possible immunomodulatory effects of pregnancy on immunity.
Replication	Data presented includes biological replicates in all experiments (always each point on a graph represents a different biological replicate), with number of samples detailed in the Fig. legends and along the text. All in vitro assays were performed at least twice with different subjects. The data presented is representative of one assay or combined data from multiple, as detailed in the figure legends. Data from serological analyses, RT-qPCR and microfiltration also included technical replicates of each of the biological samples included.
Randomization	Individuals were age-stratified, and randomly selected (computer-generated randomization) from the previously collected census data who meet the eligibility criteria and have provided written informed consent or assent (including parental consent) were enrolled in the study.
Blinding	Data shown in Fig. 2 was performed and analysed without the experimenter knowing to which group each samples belonged, and only at the time of plotting the data was each individual assigned to its group. Metabolomic data (Fig. 4 h and supTable 8 and 9) was obtained and analysed with the experimenters blinded to which group each samples belonged to. Parasite areas measured in Fig. 5g were determined by microscopists blinded to the groups the images belonged to. Var gene bio-informatic data was analysed blinded to the groups the RNAseq reads belonged to.

Reporting for specific materials, systems and methods

We require information from authors about some types of materials, experimental systems and methods used in many studies. Here, indicate whether each material, system or method listed is relevant to your study. If you are not sure if a list item applies to your research, read the appropriate section before selecting a response.

Materials & experimental systems		Methods	
n/a	Involved in the study	n/a	Involved in the study
<input type="checkbox"/>	<input checked="" type="checkbox"/> Antibodies	<input type="checkbox"/>	<input checked="" type="checkbox"/> ChIP-seq
<input checked="" type="checkbox"/>	<input type="checkbox"/> Eukaryotic cell lines	<input type="checkbox"/>	<input checked="" type="checkbox"/> Flow cytometry
<input checked="" type="checkbox"/>	<input type="checkbox"/> Palaeontology	<input type="checkbox"/>	<input checked="" type="checkbox"/> MRI-based neuroimaging
<input checked="" type="checkbox"/>	<input type="checkbox"/> Animals and other organisms		
<input type="checkbox"/>	<input checked="" type="checkbox"/> Human research participants		
<input type="checkbox"/>	<input checked="" type="checkbox"/> Clinical data		

Antibodies

Antibodies used

Surface antibodies were used at a dilution of 1:25 and are the following: CD14-PE (clone 61D3 eBioscience #12-0149-42) / -BV71 (clone M5E2 BD Biosciences #740773), CD16-BV421(clone 3G8 BD Biosciences #562874) / -BV605 (clone 3G8 BioLegend #302039) / -BV711 (clone 3G8 BD Biosciences #563127), CD19-PE Texas Red (clone HIB19, BD Biosciences #562321) / -BV421

(clone HIB19 BioLegend #302233) / -PerCPcy5.5 (clone SJ25-C1eBioscience #45-0198-42), CD21-FITC (clone BL13 Beckman Coulter #IM0473U) / -PE TexasRed (clone B-ly4 BD Biosciences #563474) / -BV421 (clone B-ly4 BD Bioscience # 562966) / -APC (clone HB5 eBioscience #17-0219-42), CD27-FITC (clone M-T271 Biolegend #356404) / -PEcy7 (clone M-T271 BD Biosciences #560609) / -AlexaFluor 700 (clone O323 Biolegend #302814) / -BV421 (clone M-T271 BioLegend #356418 / -BV650 (clone O323 BioLegend #302828) / -APCcy7 (clone O323 BioLegend #302816), CD3-BV510 (clone OKT3 BioLegend #317332) / -BV711 (clone UCHT1 BD Biosciences # 563725) / -PerCPcy5.5 (clone OKT4 BioLegend #317412) / -APC (clone RPA-T4 BD Biosciences #555349), CD8-PEcy7 (clone RPA-T8 BD Biosciences #57746) / -APCcy7 (clone SK1 BD Biosciences #557834), TCRγδ-PE (clone B1.1 eBioscience #12-9959-42), CD56-BV510 (clone HCD56 BioLegend #318340) / -BV605 (clone HCD56 BioLegend #318334). After fixing and permeabilizing the cells with FoxP3 Staining Buffer Set (eBioscience #00-5523-00) according to the manufacturer instructions, PBMCs were stained for 30 min with fluorescently labelled intracellular antibodies at a 1:25 dilution: CD25-PEcy7 (clone BC96 eBioscience # 25-0259-42), T-bet-PE Texas Red (clone O4-46 BD Biosciences #562467), IL-2-FITC (clone MQ1-17H12 eBioscience #11-7029-42), Granzyme B-PE Texas Red (clone GB11 BD Biosciences # 562462), FCRL5-PE (clone 509f6 BioLegend # 340304), Granzyme A-AF647 (clone CB9 BioLegend #507214). The secondary antibody phycoerythrin-conjugated Goat Anti-Human IgG (Polyclonal Jackson ImmunoResearch #109-116-170) diluted 1:3000 was used to detect IgG binding to PfEMP1 domains.

Validation

All antibodies used were commercially available and thus had been previously validated; and all stainings included unstained and single-color controls, as well as fluorescence minus one (FMO) controls to help define the gates and no background fluorescence or overlapping of the emission spectrum was measured, gating strategies are available in Extended Fig. 2.

Human research participants

Policy information about [studies involving human research participants](#)

Population characteristics

All study subjects will be selected from the village of Kalifabougou, Mali. Male and female volunteers 3 months to 40 years of age will be included. This age range captures the period over which immunity to malaria is acquired in areas of intense Pf transmission like Mali.

Recruitment

A random sample of the village population was drawn in an age-stratified manner to enrol in the study, including individuals aged 3 months to 45 years. The names of potential subjects were selected at random (computer-generated randomization to avoid any self-selection or other biases) from an age- and gender-stratified census (previously collected) of the entire village. The study team contacted the selected individuals in person by visiting their respective homes and inviting them to participate in the study. Written informed consent was obtained from all participants and the parents/guardians of included children.

Ethics oversight

The Ethics Committee of Heidelberg University Hospital, the Faculty of Medicine, Pharmacy and Odontostomatology (FMPOS) at the University of Bamako, and the National Institute of Allergy and Infectious Diseases of the National Institutes of Health Institutional Review Board approved this study.

Note that full information on the approval of the study protocol must also be provided in the manuscript.

Clinical data

Policy information about [clinical studies](#)

All manuscripts should comply with the ICMJE [guidelines for publication of clinical research](#) and a completed [CONSORT checklist](#) must be included with all submissions.

Clinical trial registration

The study is registered at ClinicalTrials.gov (identifier NCT01322581).

Study protocol

The protocol of the observational study "A Longitudinal Systems Biological Analysis of Naturally Acquired Malaria Immunity in Mali" can be found here: <https://clinicaltrials.gov/ct2/show/NCT01322581>

Data collection

Samples and clinical data were obtained in a cohort study conducted between 2011 and 2019 in Kalifabougou, Mali, a rural village where malaria transmission occurs from June through December. A single clinic and pharmacy provided the only access to antimalarial drugs. Clinical malaria episodes were detected prospectively by passive surveillance and were defined by axillary temperature $\geq 37.5^{\circ}\text{C}$, ≥ 2500 asexual parasites/ μL of blood, and no other cause of fever upon physical examination. Malaria episodes were treated with a standard 3-day course of artemether/lumefantrine according to national guidelines. Cross-sectional clinical visits and blood draws were performed at the beginning (January), mid (March) and end (May) of each dry season.

Outcomes

The pre-defined primary outcome of the clinical study (identifier NCT01322581 onClinicalTrials.gov) was to identify genome-wide expression profiles induced by Pf infection that are associated with immunity to malaria, and it is not related nor was it addressed in this particular manuscript. Our analyses and manuscript relate to the Exploratory Objectives of NCT01322581, to compare immune parameters in Pf-infected and -uninfected individuals at the end of the dry season to investigate host and parasite factors associated with chronic asymptomatic Pf infection. And these measures were accessed monitoring all malaria cases through passive surveillance and have all asymptomatic infection at three different times of the dry season actively monitored.

Flow Cytometry

Plots

Confirm that:

- The axis labels state the marker and fluorochrome used (e.g. CD4-FITC).
- The axis scales are clearly visible. Include numbers along axes only for bottom left plot of group (a 'group' is an analysis of identical markers).
- All plots are contour plots with outliers or pseudocolor plots.
- A numerical value for number of cells or percentage (with statistics) is provided.

Methodology

Sample preparation

For PBMCs: Freshly or immediately after thawing or after washing if used fresh, 1 - 2x10⁶ PBMCs were incubated for 30 min at 4°C with different combinations of the following fluorescently labelled surface antibodies. After fixing and permeabilizing the cells with FoxP3 Staining Buffer Set (eBioscience) according to the manufacturer instructions, PBMCs were stained for 30 min with fluorescently labelled intracellular antibodies.

For P. falciparum-specific B cell: Recently thawed PBMCs were stained with biotinylated recombinant PfMSP1 and PfAMA1 and then coupled to fluorescently labelled streptavidin (Hopp et al. in preparation), together with the following labelled monoclonal antibodies. Aqua dead cell stain was added for live/dead discrimination (Thermo Fisher Scientific).

For P. falciparum quantification: RBC pellets removed from CPT tubes after leucocyte isolation were washed and stained with 5x SYBR Green II (Invitrogen) and 7.5µM MitoTracker (Applied Biosystems) for 30 min at 37 °C. as described in the methods on the manuscript

Instrument

Data includes samples analysed using FACS Canto II, BD LSR II, LSR Fortessa or LSR Fortessa X20 flow cytometers (all from BD)

Software

FACS DIVA 8.0.2 and FlowJo 10.2 or higher versions

Cell population abundance

population abundance was determined by % of parent population, and a minimum of cells was set for some more rare populations, which did not happen often. Samples with less than 50 iRBCs when quantifying P. falciparum were not included in the analysis. PBMC samples not counting more than 500 monocytes were not included in the monocyte analyses.

Gating strategy

Gating strategies of all relevant populations are available in Extended figure 2. Doublets were excluded based on FSCh by FCSa. and from singlets total PBMC or lymphocytes were gated with FSCa by SSCa parameters. CD14 positive cell identified and total Monocytes and levels of CD16 and 14 further allowed distinguishing the different Monocyte subpopulations. B cells and T cells among lymphocytes were defined by the presence of CD3 and CD19 respectively. T cells were further subdivided in CD4 and CD8 T cells presence of those markers; and B cells divided in their subpopulations based on CD21 and CD27. Lymphocytes that had not CD19 nor CD3 were categorized as NK cells depending on their expression of CD16 and CD56. Intracellular markers present in any of the cell populations mention above identified positive populations of interest.
For P. falciparum specific memory B cell population, an additional live/dead stain was used to exclude dead cells from the singlet population together with a non-B cell marker of the same fluorescence. Mature B cells were defined based on CD19 and CD10 and the different B cell subpopulations based on CD21 and CD27 were further defined as P. falciparum or HA positive if there were double positive for biotinylated recombinant PfMSP1 or PfAMA1 and then coupled to 2 mixed fluorescently labelled streptavidin.

Tick this box to confirm that a figure exemplifying the gating strategy is provided in the Supplementary Information.